SOME STUDIES OF ION IMPLANTATION AT LOW ENERGIES

by 672

IRAJ ROJHANI

B. S., Kansas State University, 1969

A MASTER'S THESIS

submitted in partial fulfillment of the

requirements for the degree

MASTER OF SCIENCE

Department of Electrical Engineering

KANSAS STATE UNIVERSITY
Manhattan, Kansas

1970

Approved by:

Major Professor

TABLE OF CONTENTS

THIS BOOK CONTAINS NUMEROUS PAGES WITH DIAGRAMS THAT ARE CROOKED COMPARED TO THE REST OF THE INFORMATION ON THE PAGE.

THIS IS AS RECEIVED FROM CUSTOMER.

LIST OF FIGURES

FIGURE PAGE

LIST OF TABLES

INTRODUCTION

The aims of this research were two-fold. The first objective was the investigation of the performance characteristics of a commercial ion source which is to be used in the 600 KV Cockcroft-Walton Linear Accelerator presently under assembly. In order to examine the characteristics of this ion source it was assembled and used in a simple experimental system (to be discussed in Chapter IV). The advantages in using this type of ion source along with the complexities which could arise during use will be discussed in later chapters.

The second objective was a study of the behavior of various materials subjected to low (< 20 KV) energy ion implantation. Ion implantation in semiconductors is currently receiving attention in several rather different contexts. For example, semiconductor physicists and device engineers are interested in the implantation process because it provides a new doping technique with several potential advantages over more conventional doping methods. Materials scientists are interested in various characteristics of ion implanted materials, such as electrical, chemical, etc., because they provide important tools for studying diffusion processes and radiation damage effects.

The introduction of impurities into semiconductor materials to modify their conductivity and type can be carried out either chemically (e.g., thermal diffusion) or by ion implantation process. At present, the most common commercial method of semiconductor doping (thermal diffusion) is reaching the limit of its capability in, for example, the control of doping level and

junction depth when very shallow junctions are required. Much of the attractiveness of ion implantation stems from the fact that it is a non-equilibrium process, which means that the maximum local concentration of the dopant ion species is independent of the chemical solubility. This method, which has recently been adopted by a few industries as a tool for commercial production of doped semiconductor materials, thus allows distributions of impurities which differ substantially from those that can be obtained by conventional thermal diffusion techniques. Consequently, greater freedom in the choice and control of impurity concentration profiles is possible. In addition the dopant ions may be of any species which can be produced in an ion source. Also, because of the large degree of control over the ion energy, as well as the control over the substrate parameters such as temperature and orientation of target material, a high degree of regulation over the penetration depth and concentration profile of implantated ions is possible.

Naturally the advantages of ion implantation are not achieved without associated disadvantages. Particles involved in ion implantation have energies of many orders of magnitude higher than those utilized in thermally activated methods, therefore, some crystalline disorder is produced as a consequence of ion bombardment. This disorder is generally called damage. The damage can usually be repaired by annealing at temperatures (300 - 900°C) lower than those normally needed (800 - 1200°C) to introduce impurities by diffusion.

In Chapters I and II of this paper basic theories of crystals and characteristics of a p-n junction are briefly discussed. In Chapter III principles of ion implantation and important parameters associated with it are explained. The apparatus necessary for ion implantation along with the

experimental system used by the author are described and discussed in Chapter IV. Operations associated with the experimental system along with the results of ion bombardment experiments will be discussed in Chapter V. Finally, Chapter VI contains: a summary of the presented work and some conclusions concerning the performance of the commercial ion source; a discussion of the use of ion implantation techniques for doping semiconductor materials; and some preliminary measurement of the properties of ion-doped materials.

CHAPTER I

CRYSTAL THEORY

1.1 Introduction

The name "crystal" comes from the Greek word "krystallos" meaning clear ice, and was first applied to describe transparent quartz stones. The name crystal was extended to other manifestations of solids that bore the relation to the original rock crystal of being bounded by many flat shiny faces, symmetrically arrayed. A crystal is a regular array of atoms arranged in some repetitive pattern. The most important property of a perfect crystal* is that if the relative positions of a small number of atoms are known, the positions of all the other atoms in the crystal can be determined. This basic feature of all crystal is the regularity of their atomic arrangement. However, periodic patterns are not the exclusive property of crystals.

1.2 Crystal Structure

In order to have a better understanding of diffusion processes, which are basic methods of semiconductor doping, some knowledge of the geometric arrangement of atoms in crystals is necessary. For a crystalline solid there exist three primitive basis vectors[1], $\underline{a}$, $\underline{b}$, $\underline{c}$, such that the crystal structure remains invariant under translation through any vector which is the sum of

---

* A perfect crystal is one which is free of any flaws or imperfections.

integral multiples of these basis vectors. In other words, the lattice sites (direct)* can be defined by the set

$$\underline{l} = n_1\underline{a} + n_2\underline{b} + n_3\underline{c} \qquad (1)$$

where n_1, n_2, and n_3 are integers, and $\underline{a}$, $\underline{b}$, and $\underline{c}$ are direct basis vectors.

Crystals may be classified into seven basic systems. These are called triclinic, monoclinic, orthorhombic, trigonal, tetragonal, hexagonal, and cubic. From these seven systems the cubic system, in which the basis vectors $\underline{a}$, $\underline{b}$, and $\underline{c}$ are equal and perpendicular to each other, constitutes the basic structures of the majority of semiconductor solids. The three common arrangements of the atoms in this system are primitive cube (pc), body-centered cube (bcc), and face-centered cube (fcc). Figure 1-1 shows these arrangements in the form of unit cells (direct lattice).

A great many of the important semiconductor materials have the diamond or zincblende lattice structure. They are covalently bonded materials, and due to the strongly directional properties of the covalent bond each atom in a crystal of carbon, silicon, or germanium has four nearest neighbors, joined at tetrahedral angles. The resulting structure can be described as face-centered cubic; effectively it is two f.c.c. lattice displaced by (¼, ¼, ¼). In Fig. 1-2 (a) and 1-2 (b) three dimensional representations of diamond and zincblende crystal structures are illustrated respectively. For the diamond lattice, such as silicon (Si) or germanium (Ge), all the atoms are either silicon atoms or all are germanium atoms, respectively, whereas in a

---

* Direct lattice here is in contrast to reciprocal lattice, which will be discussed later.

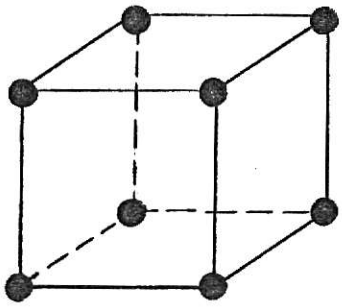

(a)

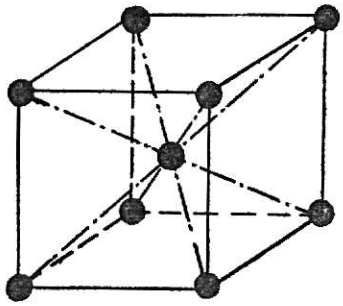

(b)

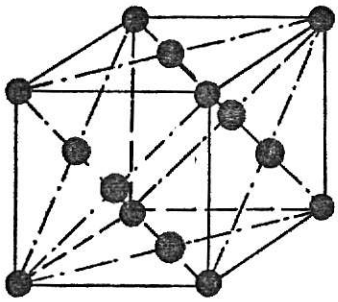

(c)

Figure 1-1. Some of the important unit cells.
(a) Simple Cubic. (b) Body-Centered Cubic.
(c) Face-Centered Cubic.

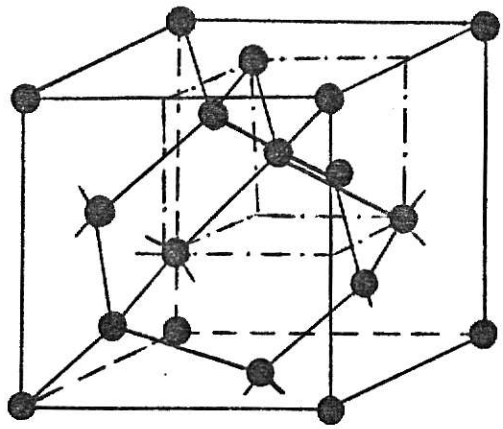

(a)

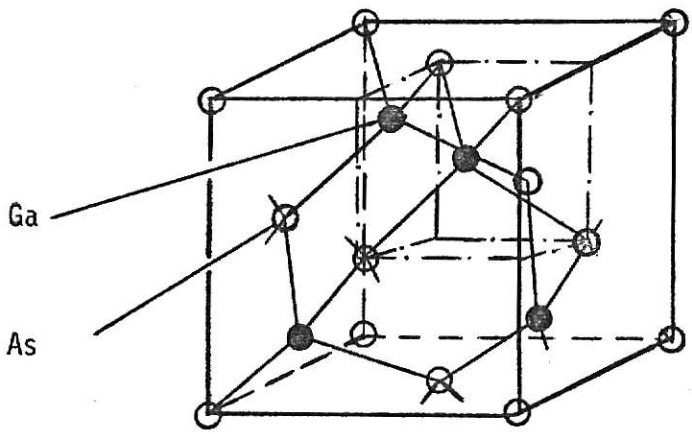

(b)

Figure 1-2. Three-dimensional representations of (a) diamond and (b) zincblende crystal structures.

zincblende lattice, such as gallium arsenide (GaAs), one of the f.c.c. sublattices is gallium and the other is arsenic.

1.3 Crystal Orientation

A convenient method of defining the various planes in a crystal is by the use of the Miller indices which are determined by first finding the intercepts of the plane with three basis axes in terms of the lattice constants and then taking the reciprocals of these numbers and reducing them to the smallest three integers (having the same ratio). The result is enclosed in parentheses (hkl) as the Miller indices for a single plane or a set of parallel planes[3]. Miller indices of the lowest index planes, which are important in semiconductor fabrication, are shown in Fig. 1-3.

The importance of Miller indices and reciprocal lattice vectors will become more evident when we study the structural characteristics and flaws by electron microscopy (electron diffraction).

1.4 Reciprocal Lattice Vectors

For a given set of direct basis vectors, one can define a set of reciprocal lattice basis vectors, a*, b*, c* such that

$$a^* = \frac{\underline{b} \times \underline{c}}{\underline{a} \cdot \underline{b} \times \underline{c}}$$

$$b^* = \frac{\underline{c} \times \underline{a}}{\underline{b} \cdot \underline{c} \times \underline{a}} \qquad (2)$$

$$c^* = \frac{\underline{a} \times \underline{b}}{\underline{c} \cdot \underline{a} \times \underline{b}}$$

where

$$\underline{a} \cdot \underline{b} \times \underline{c} = \underline{b} \cdot \underline{c} \times \underline{a} = \underline{c} \cdot \underline{a} \times \underline{b} = V_d \qquad (3)$$

where V_d is the volume of a unit cell of the direct lattice. Therefore, the general reciprocal lattice vector can be written in the following form

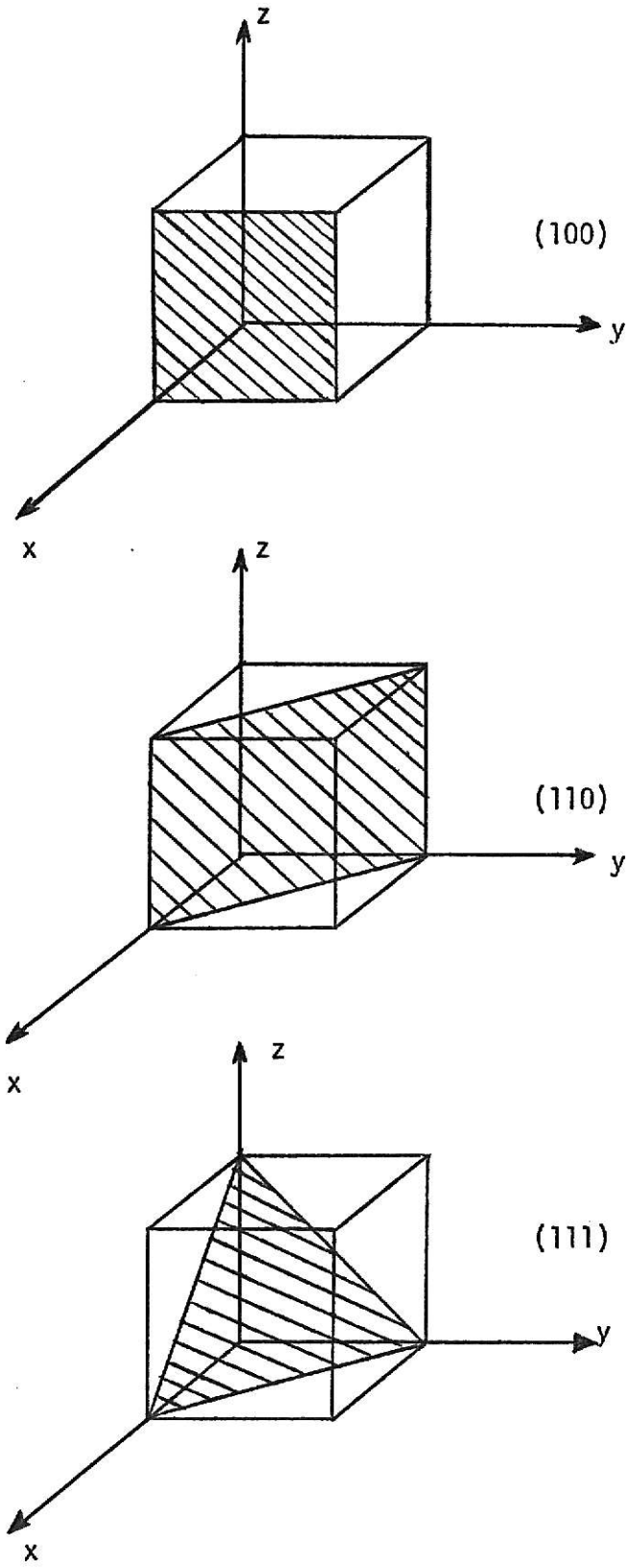

Figure 1-3. Miller indices of some important planes in a cubic crystal.

$$\underline{g} = ha^* + kb^* + lc^* \qquad (4)$$

where h, k and l are integers.

1.5 Energy Bands

The energy band structure of a crystalline solid, i.e., the energy-momentum (E-k) relationship[2] is one of the important aspects which must be considered. One notices that for any semiconductor there is a forbidden energy region in which no allowed states can exist. Above and below this energy gap are permitted energy regions or energy bands. The most important parameter in semiconductor physics is the band gap energy, E_g, which is the separation between the energy of the lowest conduction band, and that of the highest valence band. The upper bands of the forbidden region are called the conduction bands; the lower bands, the valence bands.

At room temperature and under normal atmosphere, the values of the band gap energies of the three mostly used semiconductor materials silicon (si), germanium (ge), and gallium arsenide (GaAs) are 1.12 eV, 0.803 eV, and 1.43 eV, respectively. The above values are for high-purity materials. For highly-doped materials the band gaps become smaller. Experimental results show that the energy band gaps of most semiconductors decrease with increasing temperature, and therefore, their conductivities increase[2,4]. In fact, the conductivity, σ, is proportional to an exponential function

$$\sigma \propto \exp \{ -E_g / 2kT \}$$

where E_g is the width of the gap between the filled and the empty bands, k is the Boltzman constant, and T is the temperature. Figure 1-4 shows a simplied band diagram. In Fig. 1-5 the energy band gaps of Ge, Si, and GaAs as a function of temperature are illustrated.

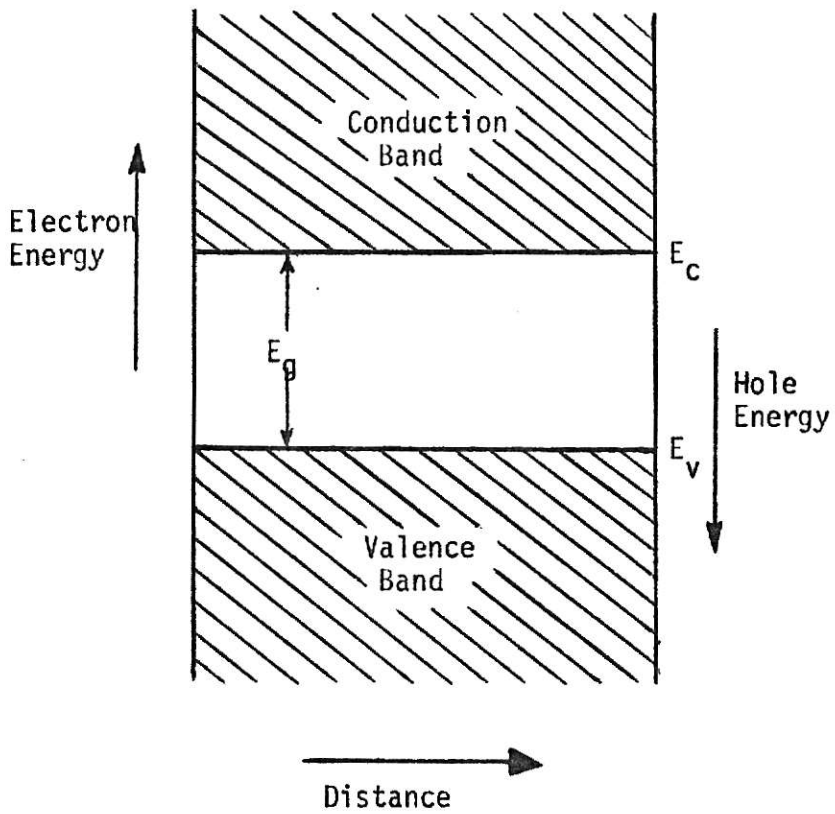

Figure 1-4. Simplified band diagram (E_c is the bottom of conduction band, E_v is the top of valence band).

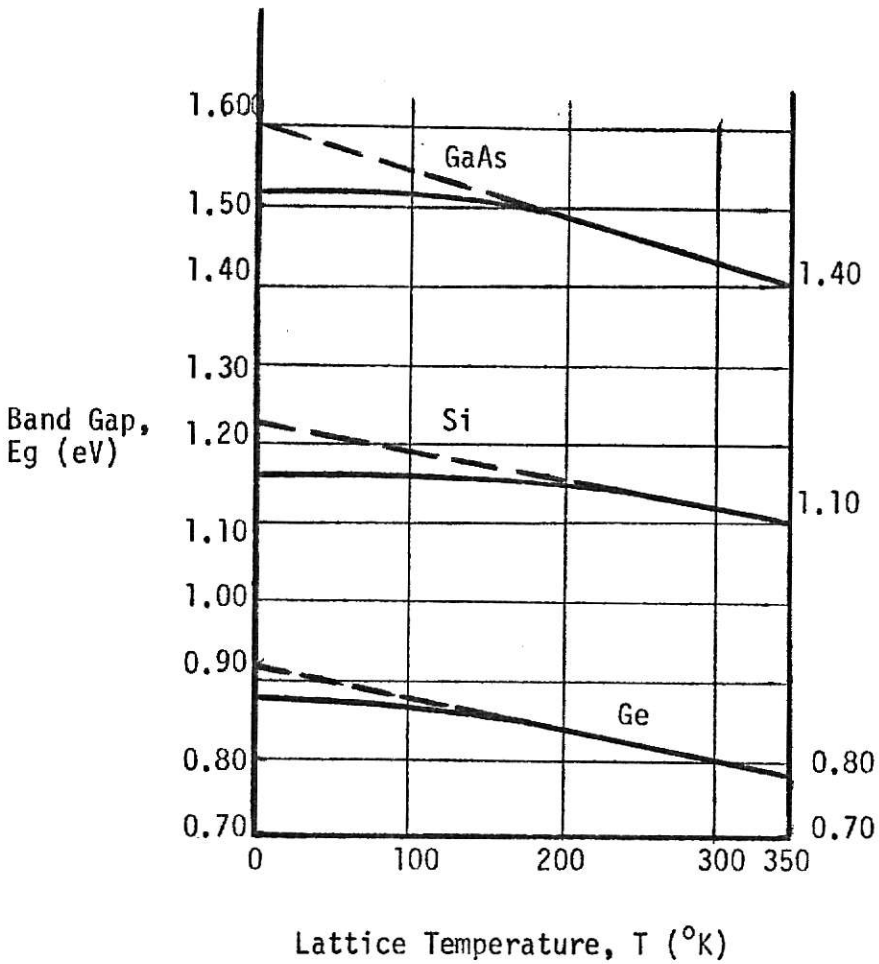

Figure 1-5. Energy band gaps of Ge, Si, and GaAs as a function of temperature. (After Smith, Ref. 5; and Neuberger, Ref. 6.)

It is obvious from the above discussion that the electrical properties of a semiconductor depend strongly on temperature because the number of electrons excited across the forbidden energy gap increases rapidly as the temperature is increased.

The presence of a very small concentration of foreign atoms can have a profound effect on the concentration of electrons in the band above the forbidden energy gap. Fermi level, or Fermi energy, E_F, which gives an explanation for the distribution of electrons among the various bands in crystals, is a very useful and convenient parameter for expressing the properties of semiconductor crystals. In a metal, for example, in which the number of levels exceeds the number of electrons because there is no forbidden energy gap, the levels are filled up to that labeled E_F. Specifically, E_F is the highest level occupied by electrons when the metal is at the absolute zero of temperature[7].

1.6 Perfection and Imperfection in Crystals

Most semiconductor devices are fabricated from single crystals, since although polycrystalline specimens can easily be grown free of impurities the grain boundaries act as undesirable sources of many mid-gap levels[7]. Thus industrial manufacturers of devices have been required to utilize the various well known crystal growing techniques (Czochralski, float-zone, crucibleless pulling, etc.) to produce single crystals of the semiconductors.

In our previous discussions of the properties of crystals we have assumed an ideal, or perfect single crystal. This is basically a theoretical concept. We must now consider a real single crystal, and we shall find that even if it is substantially free of impurity atoms, it can still contain imperfections. Most of these imperfections will have arisen during the growth process.

Imperfections or defects can be classified in three catagories. These are (1) point defects, (2) line defects, and (3) plane defects. If the deviation from a periodic arrangement, imperfection, is localized to the vicinity of only several atoms, it is called a point imperfection or a point defect. Point imperfections in crystals are generally catagorized in three different groups. These are Interstitial defects, Schottky defects, and Frenkel defects. An interstitial defect may be described as the presence of an extra atom in an interstitial site. When an atom is missing from its correct site the defect is referred to as Schottky defect. However, when an atom is displaced to an interstitial site creating a vacancy then this combination (i.e. Schottky plus interstitial) is called a Frenkel defect. The point defects are shown in Fig. 1-6.

On the other hand, if the deviation from the periodic arrangement extends throughout some regions in the crystal, it is called a lattice imperfection, for it produces a discontinuity in the lattice. The line defects may be described in forms of Edge and Screw dislocations. The edge dislocation can be defined as a row of atoms marking an edge of a crystallographic plane extending only partly into the crystal. Figure 1-7 is a three-dimensional illustration of the edge dislocation. The screw dislocation, which was introduced by Burgers (1939), consists of a line of atoms each of which has the correct number of atoms coordinating it; however, the coordination polyhedron is distorted. The screw dislocation may be clearly seen in a three-dimensional representation as is shown in Fig. 1-8.

Other defects in crystals can often be explained in terms of three fundamental defects. For example, lineage, or low angle grain boundaries can be considered as an array of well-separated edge dislocations. An "ordinary"

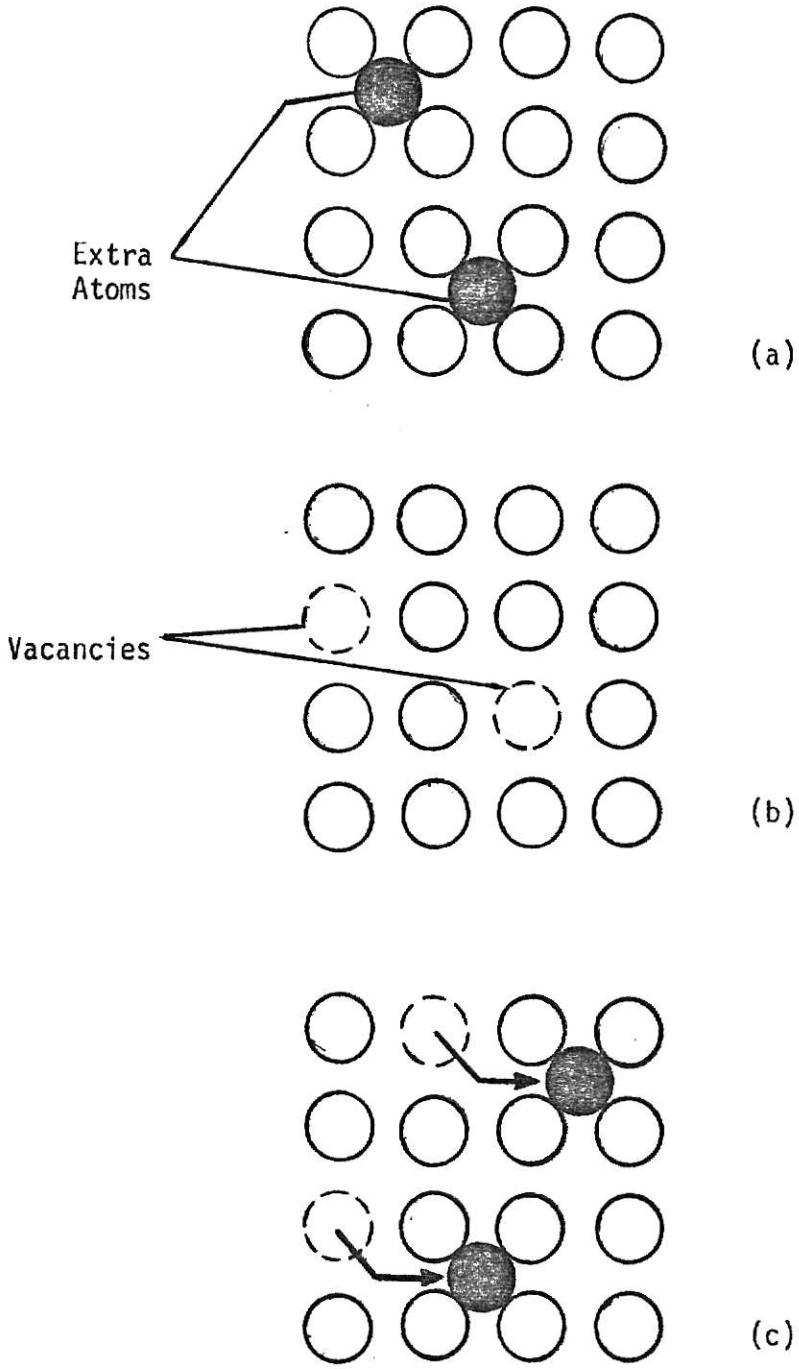

Figure 1-6. Point imperfections in crystals. (a) Interstitial defect. (b) Schottky defect. (c) Frenkel defect.

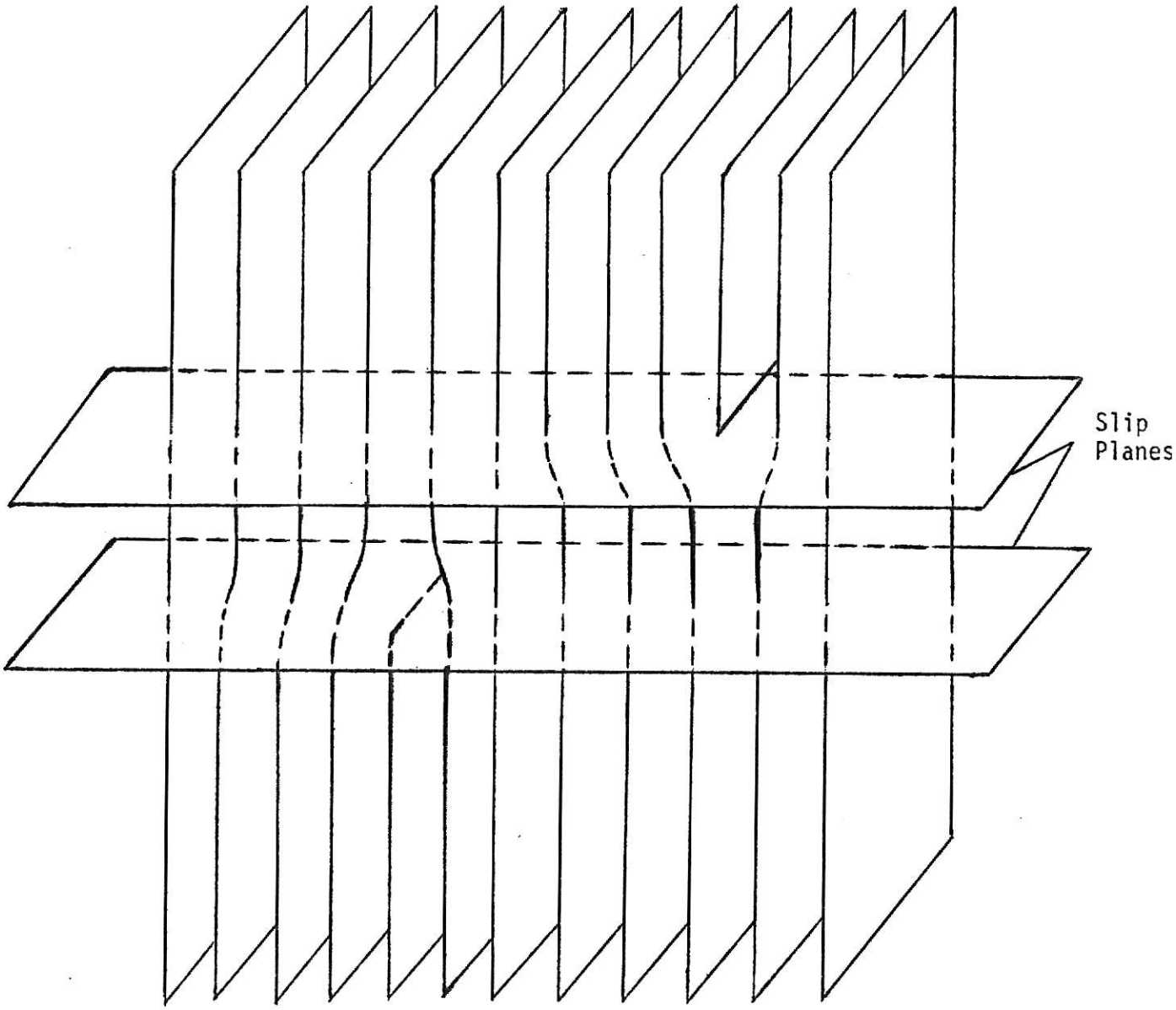

Figure 1-7. Three-dimensional representation of two edge dislocations of opposite signs.

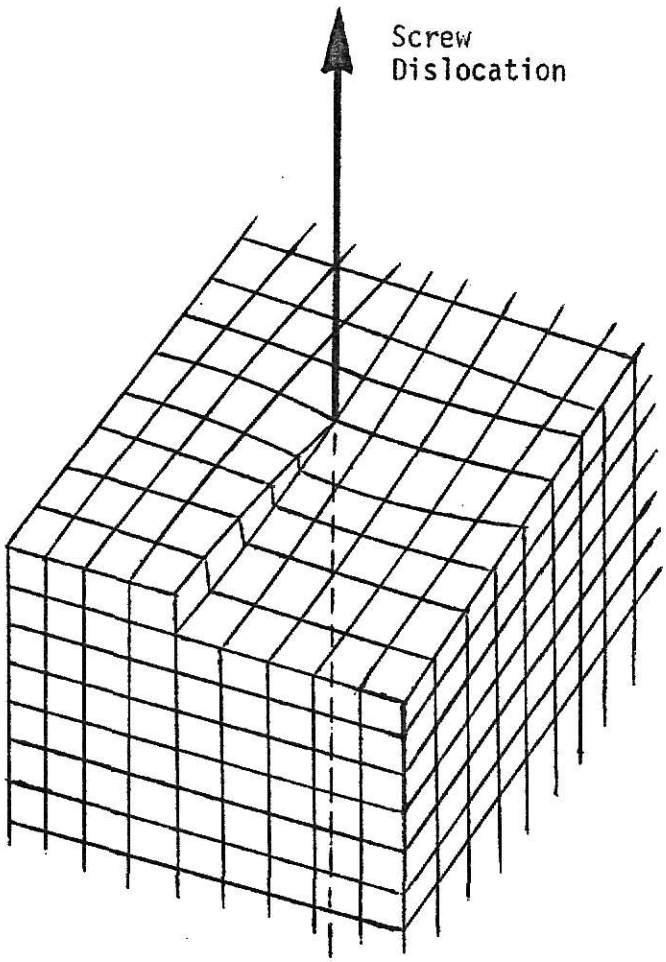

Figure 1-8. Three-dimensional illustration of screw dislocation.

grain boundary can be considered as a network of edge, or screw, or mixed dislocations.

One other defect encountered with close-packed materials is the stacking fault, which is a planar defect caused by violation of the correct stacking sequence across the {111}, close-packed planes.

1.7 Conduction in Crystals

Conductivity in crystals can be defined in terms of the number of conduction electrons n_c by the following equation

$$\sigma = n_c \, e \, \mu \tag{5}$$

where μ is the mobility and is equal to the drift velocity per unit field (drift velocity is the velocity component parallel to the applied field direction) and e is the electronic charge. Under an externally applied electric field, the free electrons in a crystal gain sufficient additional energy to move into higher unoccupied quantum states, provided that the Pauli exclusion principle is not violated. In an intrinsic semiconductor*, the electrons occupying quantum states in the conduction band move into adjacent unoccupied quantum states and the electrons remaining in the valence band can move into the quantum states that have been vacated by the thermal excitation of electrons to the conduction band[3].

Since in a crystal, depending whether it is an n-type semiconductor or a p-type semiconductor (to be discussed later) majority carriers are electrons or holes, respectively, the conductivity of the semiconductor can be expressed by

$$\sigma = en \, \mu_n + ep \, \mu_p \tag{6}$$

---

* Intrinsic semiconductor is a crystal in which the temperature at which conductivity becomes appreciable depends on the width of the forbidden band which, in turn, depends on the crystal structure.

where n is the density and μ_n the mobility of electrons occupying states in the conduction band, and p is the density and μ_p the mobility of the holes. In an intrinsic semiconductor the number of electrons occupying states in the conduction band equals the number of holes or unoccupied states in the valence band, so that

$$n_c = 2n = 2p$$
$$\mu = \tfrac{1}{2} (\mu_n + \mu_p). \qquad (7)$$

1.8 Diffusion In Crystals

The diffusion process is based on two different mechanisms. Many investigators favor the vacancy mechanism although there are reasons for expecting that the interstitial mechanism may be important. The presence of point defects in a crystal allows diffusion to take place without producing the large local distortions which are involved in direct interchange. Crystals with the diamond structure, such as silicon and germanium, differ from metalic and ionic crystals in two important related respects. Firstly, the forces holding the atoms together are directional; each atom is at the center of a tetrahedron, the bonds of which are directed toward the tetrahedron corners. Secondly, in tetrahedral binding the crystal structure is quite open[4]. Therefore, the interstitial spaces are quite large. These two facts, the directionality of the bonds and the openness of the structure, have a profound effect on diffusion.

CHAPTER II

THE p-n JUNCTION

2.1 Introduction

Conduction in semiconductors can take place by movements of either electrons or holes. If the carrier type is changed abruptly by some means the resulting structure is known as a p-n junction. The formation of a p-n junction, its electrical properties (of which rectification is the obvious one), and some other properties which may be explained with the aid of energy band models will be discussed in this chapter.

2.2 p-Type Material

If a crystal is doped with an excess of acceptor-type impurity atoms, so that the holes become the majority carriers, it is called a p-type semiconductor. Thus, should the impurity atom contain only three electrons in its valence band, all three will be used up in covalent bonds with neighboring semiconductor atoms. Since a lack, or deficiency, of one electron prevails an empty space will exist causing one bond to be unsatisfied. This empty space in the impurity atom's valence band, which is called a hole, is positive in nature. As such, it is able to accept an electron from the crystal in order to satisfy the incomplete bond. The gaining of an electron upsets the acceptor's charge balance causing it to ionize. Since, the holes predominate in this material, p-type, the majority carriers become holes.

2.3 n-Type Material

A crystal is called an n-type semiconductor when electrons predominate and they become the majority carriers. When the impurity atom contains five electrons in its valence band, four will be used to form covalent bonds with neighboring semiconductor atoms. The fifth electron is extra. Therefore, this extra electron is free to leave its parent atom. With the loss of the electron the donor's charge balance is upset causing it to ionize. Since the electrons (majority carriers) greatly outnumber the holes, the crystal is negative in nature.

2.4 p-n Junction "Formation"

The word formation appears in quotes in the heading for this section because what it is meant to describe here is not an actual fabrication process but instead the basic nature of the equilibrium condition one finds in a p-n junction. A junction could theoretically be produced by aligning two silicon crystal faces, one p-type and one n-type, so that the regular array of silicon atoms of crystallographic structures continued undisturbed across the boundary. However, in reality no such interaction would be physically possible, and in order to form a p-n junction one has to start with one type material, e.g. p-type or n-type, and build up the other type on the surface of the first one. This process is possible by different techniques such as thermal diffusion and ion implantation.

We may expect the following interactions to take place at the boundary. There will be some mobile and some immobile charges in both samples. The mobile charges will cause transient flows of holes and electrons across the boundary. More specifically, holes will diffuse from the p-type into n-type while electrons will diffuse in the opposite direction. The flows are shown in Fig. 2-1.

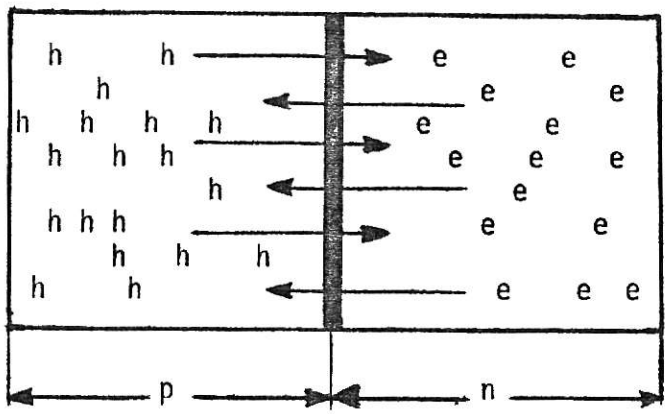

Figure 2-1. Transient hole-electron diffusion in a p-n junction.

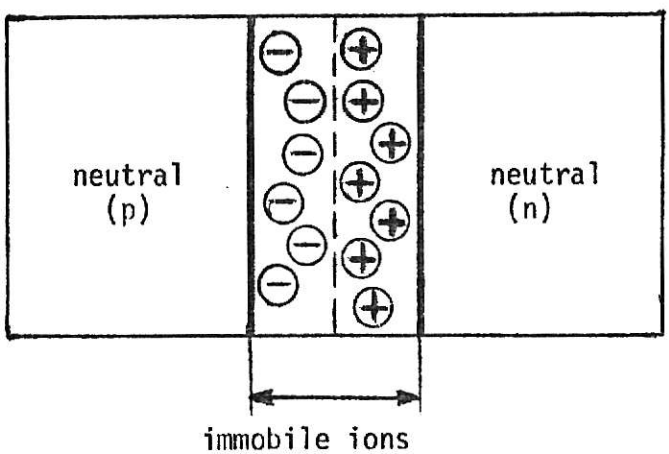

Figure 2-2. Space charge region in a p-n junction.

The diffusion of these carriers produces a charge unbalance. Consider the p-side, for example. As it gives up holes to the n-side a net negative charge due to ionized acceptor atoms is left behind. In addition, electrons coming in from the n-side recombine with holes, so further upsetting the balance between holes and acceptors. Thus near the boundary there will be a layer of acceptor ions with no free holes or electrons. This region will contain a net negative charge in the form of immobile ions. Similarly there will be a positively charged region, which contains donor ions with no free holes or electrons, in the n-type material. This pair of charged regions, which is called the "space charge layer", is shown in Fig. 2-2.

There will be an electric field associated with the charge unbalance existing in the space charge layer. This field, being directed from right to left (see Fig. 2-2) produces conduction flows which are opposite to the diffusions. Thus the net charge flows decrease in magnitude as the charge unbalance builds up. Finally a thermal equilibrium is reached in which the charge unbalance becomes large enough that the conduction and diffusion flows become equivalent and therefore cancel each other's effect and no additional charge unbalance is produced. The energy band diagrams, before and after equilibrium is reached, are given in Fig. 2-3. The amount of change in the energy level in the space charge layer is E_0 (see Fig. 2-3). This change occurs because the electric field in the space charge layer causes the electric potential and the corresponding electron potential energy to vary with the distance in this region. This energy differance, E_0,is known as the barrier energy. Therefore, we can relate the potential difference across the space charge region, barrier potential, V_0, and E_0 in the following manner

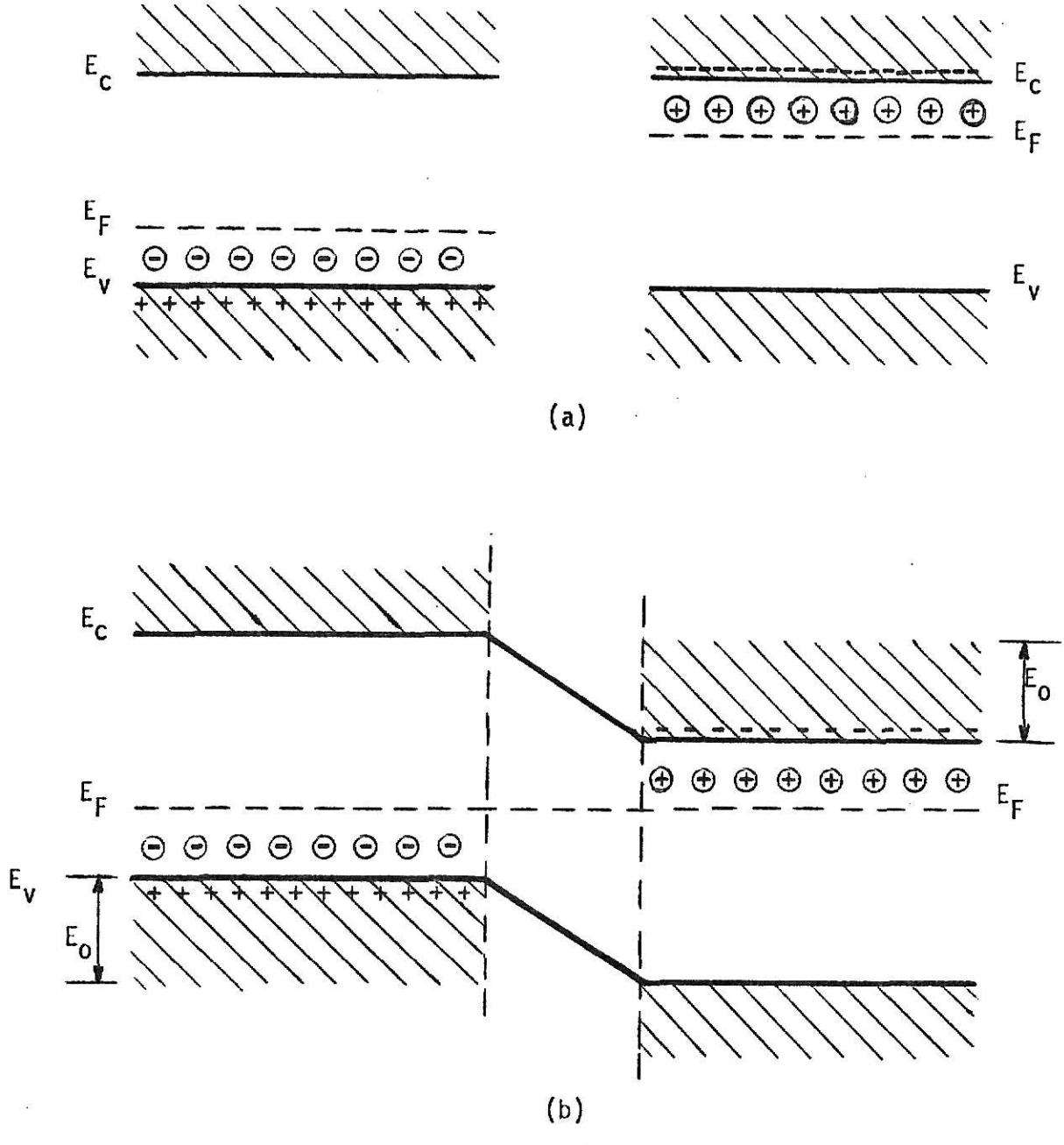

Figure 2-3. Energy band diagrams (a) before interactions start, (b) after equilibrium is reached (constant Fermi level, E_F).

$$V_o = \frac{E_o}{q} \tag{8}$$

where q is the electronic charge.

2.5 Junction Breakdown

When a sufficiently high field is applied to a p-n junction, the junction "breaks down" and conducts a very large current. There are basically three breakdown mechanisms: the thermal instability, the tunneling effect, and the avalanche multiplication[2].

2.5.1 Thermal Instability. The breakdown due to thermal instability is responsible for maximum dielectric strength in most insulators at room temperature, and is also a major effect in semiconductors with relatively small band gaps (e.g., Ge). Because of the dissipation which is caused by the reverse current at high reverse voltage, the junction temperature increases. This, in turn, increases the reverse current. This effect is called thermal instability, and if it continues will destroy the junction.

2.5.2 Tunneling Effect. When the field increases at the junction, significant current begins to flow by means of the band -to- band tunneling process. In order to obtain a high field the junction must have relatively high impurity concentrations. The tunneling effect would cause breakdown voltages less than about $4E_g/q$, where E_g is the gap energy and q is the magnitude of the electronic charge. The tunneling effect is shown in Fig. 2-4.

2.5.3 Avalanche Multiplication. The most important mechanism in junction breakdown is the avalanche multiplication (or impact ionization). The avalanche breakdown voltage imposes an upper limit on the reverse voltage for most p-n junctions (diodes) and on the collector voltage of all transistors[2].

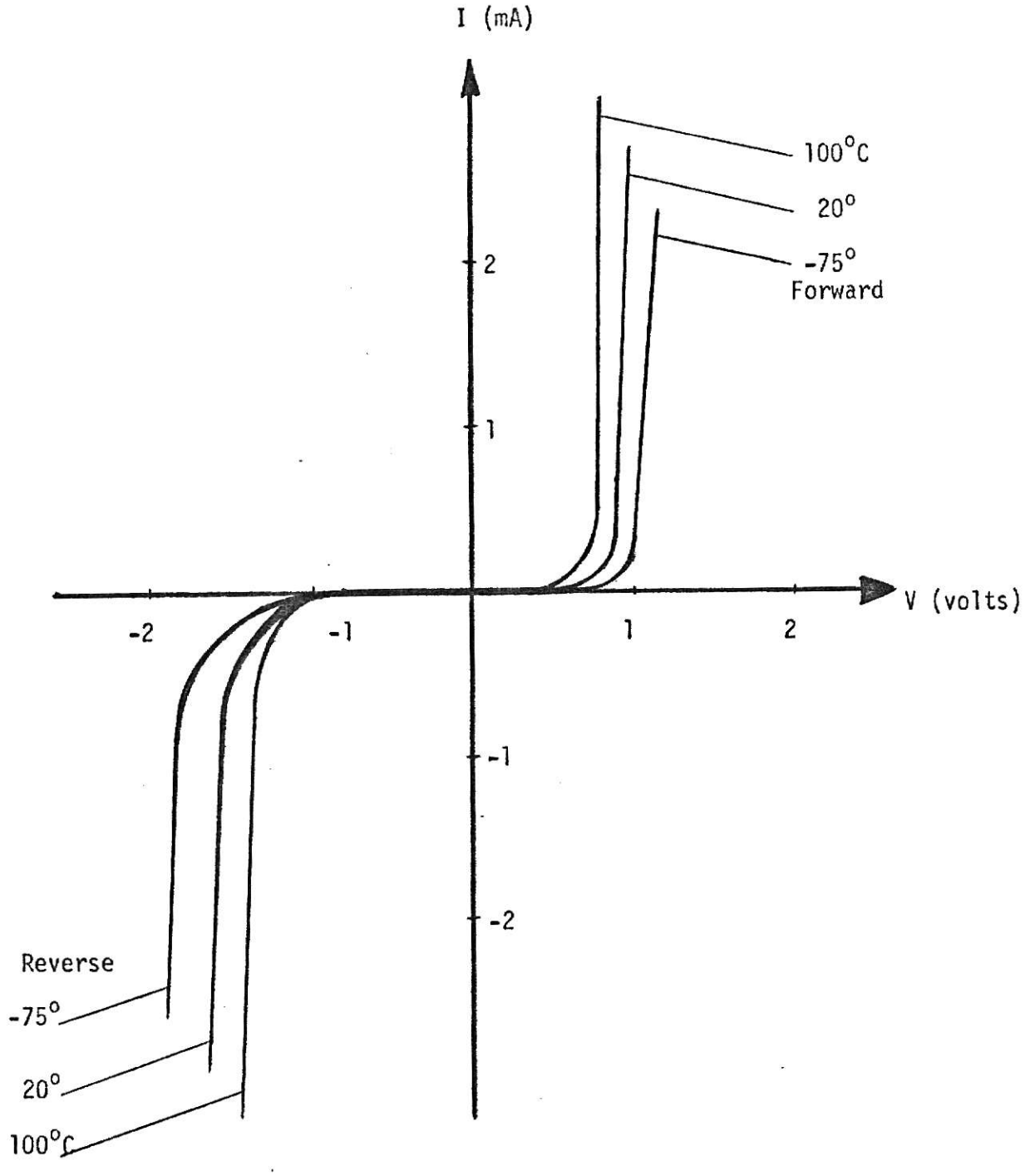

Figure 2-4. Voltage-current characteristic of tunneling breakdown. (After Strutt, Ref. 7).

2.6 Junction Capacitance

The junction (depletion-layer) capacitance per unit area is defined as

$$C_j = \frac{dQ_c}{dV} \tag{9}$$

where C_j is junction capacitance, and dQ_c is the incremental increase in charge per unit area upon an incremental change of the applied voltage dV. In other words, the junction capacitance can also be defined by

$$C_j = A\left(q\ \varepsilon \frac{N}{2}\right)^{\frac{1}{2}} \ (V_o - V)^{-\frac{1}{2}} \tag{10}$$

where A is the cross-sectional area, ε is the electric permittivity, V_o is the barrier potential, V is the applied voltage, and N is defined as follows, with N_a and N_d the acceptor and donor concentration, respectively[9]

$$N = \frac{1}{\frac{1}{N_a} + \frac{1}{N_d}} = \frac{N_a N_d}{N_a + N_d} . \tag{11}$$

It is seen from Eq. (10), that the junction capacitance can be controlled by the applied voltage, V. This voltage controlled capacitance finds important applications in communication circuits where it is desired to adjust the resonant frequency.

CHAPTER III

ION IMPLANTATION PRINCIPLES

3.1 Introduction

Impurities may be introduced into semiconductors in order to modify their conductivity. This can be carried out chemically by a number of techniques, the most common of which is thermal diffusion. In this process the sample is heated in an atmosphere containing the required impurity in gaseous form. For the majority of devices that are now produced the conventional techniques are quite adequate. However, the present technology is reaching the limit of its capability for the production of a number of devices in which the doping level or junction depth has to be controlled stringently, or where very shallow junctions are required and a veriety of dopant species are to be used.

Ion implantation is an alternative means of introducing impurities into semiconductors. Ions of the required impurity are produced at a source, extracted and focussed into a beam, and then accelerated to impinge on and penetrate into the crystal to be doped[10]. There exists a number of potential advantages in the ion implantation technique, and therefore this method is currently receiving considerable attention, with regard to both fabrication techniques and the understanding of the properties of ion doped layers.

The idea of doping semiconductors by implanting suitable ions appears to have been initiated by R. S. Ohl (1952)[11], and in 1954 Shockley filed a patent in which he foresaw the use of ion beams to produce highly controlled semi-

conductor materials. The theory of the penetration of atomic particles through matter, which was treated in detail by Bohr (1948)[12], has been extensively developed by Lindhard, Scharff and Schiott (1963, LSS theory)[13] for amorphous target materials (see later).

3.2 Penetration of Ions and Range Distribution Theory

An ion with a given energy entering a target material will lose its energy through collisions with the target nuclei and electrons, and will finally come to rest. The total distance that the ion travels before coming to rest is called its "range". If this distance is projected on to the axis of the incidence beam then it is called "projected range".

The range distribution and penetration of the doping ions in semiconductor materials is of first importance. In relation to the range distribution there are several parameters which must be considered. In a typical case, the target material is known and we want to know what range distribution we can expect for a given beam in which the masses and energies of the incident particles are also known. There generally are two types of energy loss: one occurs when the incident ion and host atoms of the target collide, and the other occurs when the incident ions and host electrons interact. As Lindhard[14] points out, both electronic and nuclear stoppings* must be taken into account, and the total energy loss from both processes may be of similar orders of magnitude. Although

---

* Electronic and nuclear stoppings are also sometimes referred to as electronic and nuclear stopping powers.

these two interactions occur simultaneously they may be considered separately.

For each incident ion the energy loss theory is based on the formula

$$-\frac{dE}{dR} = NS \tag{12}$$

where $\frac{dE}{dR}$ is the average energy change per unit path length, and hence is negative for energy loss, N is the number of scattering centers per unit volume and S is the stopping cross section per scattering center. Let $S_e(E)$ and $S_n(E)$ be the electronic and nuclear stoppings respectively, then, if these are independent of each other, we can write

$$-\frac{dE}{dR} = N\left[S_e(E) + S_n(E)\right] . \tag{13}$$

From Eq. 13 the range can then be derived by integration

$$-R(E) = \frac{1}{N}\int_{o}^{E_o} \frac{dE}{S_e(E) + S_n(E)} \tag{14a}$$

or

$$R(E) = \frac{1}{N}\int_{E_o}^{o} \frac{dE}{S_e(E) + S_n(E)} \tag{14b}$$

where R(E) is the average range along the ion path. In the following two subsections electronic and nuclear stoppings will be discussed.

3.2.1 Electronic Stopping

When the incident charged particle has a very high velocity the energy loss to the target electrons is completely dominant. This extra energy loss to electrons is actually correlated to the nuclear collisions (Eq. 13), and in close collisions considerable ionization will take place (LSS model)[13].

In this model the specific energy loss is given as $N \cdot S_e(E)$, where N is the number of atoms per unit volume and $S_e(E)$ the electronic stopping. At high velocities $S_e(E)$ increases with decreasing particle velocity and it reaches a maximum value of v_1 for $v_1 \approx v_0 z_1^{2/3}$, where v_0 is Bohr velocity and z_1, the atomic number of the incident particle. For ion implantation doping of semiconductors masses and energies of incident particles are generally such that their velocity v is low, i.e., $v < v_0$. Lindhard assumes $o < v < v_1$ and his theoretical considerations lead to a velocity proportional to the electronic stopping, $v \propto S_e(E)$.

3.2.2 Nuclear Stopping

At the low energies nuclear stopping dominates over electronic stopping. Since the energy transfer in individual collisions can be quite large, the slowing- down by nuclear collisions cannot always be considered as a nearly continuous process. It is, therefore, important to know the differential scattering cross section of the target material, which is represented by $d\sigma_n$. This differential scattering cross section may be related to the average square fluctuation in energy loss (See appendix A)

$$(\overline{\Delta E})^2 = N\, dR \int T^2\, d\sigma \qquad (15)$$

where T is the energy transfer to atoms and atomic electrons, N is the number of scattering centers per unit volume, and dR is the differential target thickness.

Figure 3-1 shows the theoretical nuclear stopping (Thomas-Fermi), approximate nuclear stopping, and the electronic stopping. In this figure the following relations hold for the nuclear and the electronic stoppings

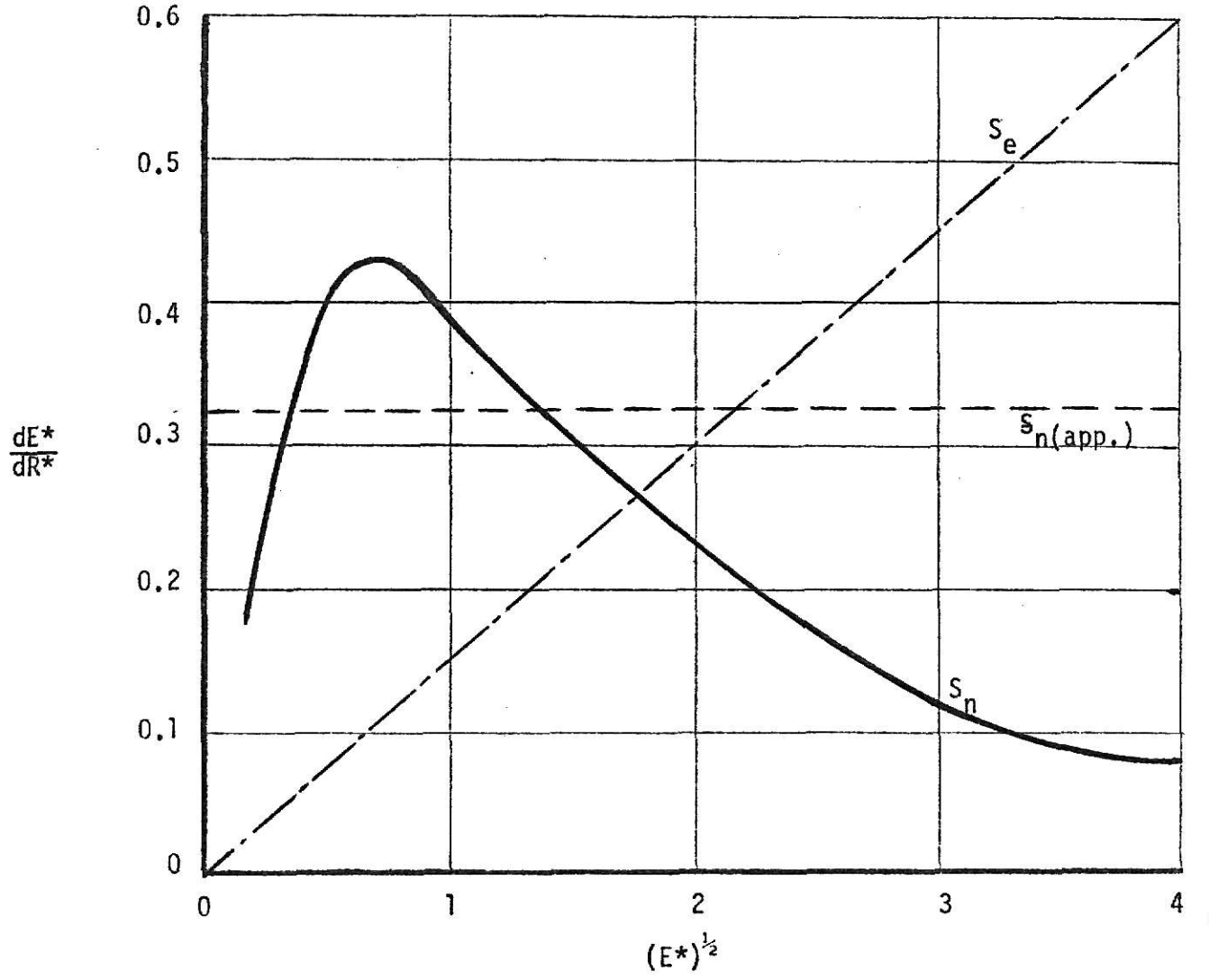

Figure 3-1. Nuclear and Electronic stoppings. The full-drawn curve is the theoretical (Thomas-Fermi) nuclear stopping (S_n), the dashed-horizontal line is an approximation of S_n, and the dash-dotted line is the electronic stopping (S_e). (After Lindhard et al. Ref. 13.)

$$S_n(E) = \left(\frac{dE^*}{dR^*}\right)_n = \int_0^{E_0} \frac{f(x)}{E^*}\, dx \qquad (16a)$$

$$S_e(E) = k \cdot (E^*)^{\frac{1}{2}} \qquad (16b)$$

where f(x) is a function of the scattering cross section, and k is a constant containing atomic numbers of incident and target atoms. (For further description see appendix A.)

3.3 Range Distribution In Amorphous And Single-Crystals

Most of semiconductor materials used in practice are in the form of single crystals, and the periodic arrangement of the atoms modifies extensively the penetration of the ions. A very common type of semiconductor crystal structure is the diamond structure which is shown in Fig. 1-2(a). If, for example, a parallel beam of light is directed through a crystal model of diamond and the light is allowed to fall on a screen, then various shadow patterns are generated according to the angle the model makes with the incident beam[10]. It is observed that the most "open" direction for the diamond structure is the <110> direction. If the incident beam is directed along a <110> axis a "channeling" effect would be observed. The channeling effect is a consequence of the crystal structural orientation, atomic openness, which also alters the possibilities of close collisions of ions with target atoms. Other crystal directions, such as <111> and <100>, also show channels although they are less "open" than the <110> direction.

To have a better understanding of the channeling effect a discussion of range-energy relations and range distribution in single crystal will follow.

Considering Eq. 14b, which is repeated below for convenience, a relation between the range of ion penetration and the ion's energy is obtained

$$R(E) = \frac{1}{N} \int_{E_o}^{o} \frac{dE}{S_e(E) + S_n(E)} . \qquad (14b)$$

This relation depends on electronic and nuclear stoppings. Figure 3-2 is a universal range-energy plot in which the theoretical curve of Thomas-Fermi in addition to a few other curves for different values of the constant k are given (see Eq. 16b).

Range distribution in single-crystal targets are different from those in amorphous targets because of the possibility of channeling effects in single-crystals. First, let us investigate the ion range distribution in amorphous targets. When $S_e(E)$ and $S_n(E)$ are known for an amorphous target, they can be substituted into the basic energy loss equation (see Eqs. 13 and 14) and the total range or total distance traveled by a projectile before it comes to rest can be computed. From Eq. 14 it is very simple to calculate the total range. However, this is not usually the quantity that is measured experimentally. Rather, the quantity which is normally measured experimentally is the projected range. Due to collisions that the incident ion makes with the host atoms, there will be some deviations in this measured quantity. From the mean and standard deviation of the projected range ($\overline{R}_p$ and $\overline{\Delta R}_p$) Gibbons[15] constructs the "Gaussian" ion distribution profile resulting from ion implantation into a known amorphous target. This Gaussian profile is shown in Fig. 3-3. In this figure $N = \frac{Q}{q}$ atoms/cm^2 where N is the number of ions in atoms/cm^2, Q is the total implanted charge in coulombs per square centimeter, and q is the electronic charge. N_p is the peak concentration of implanted

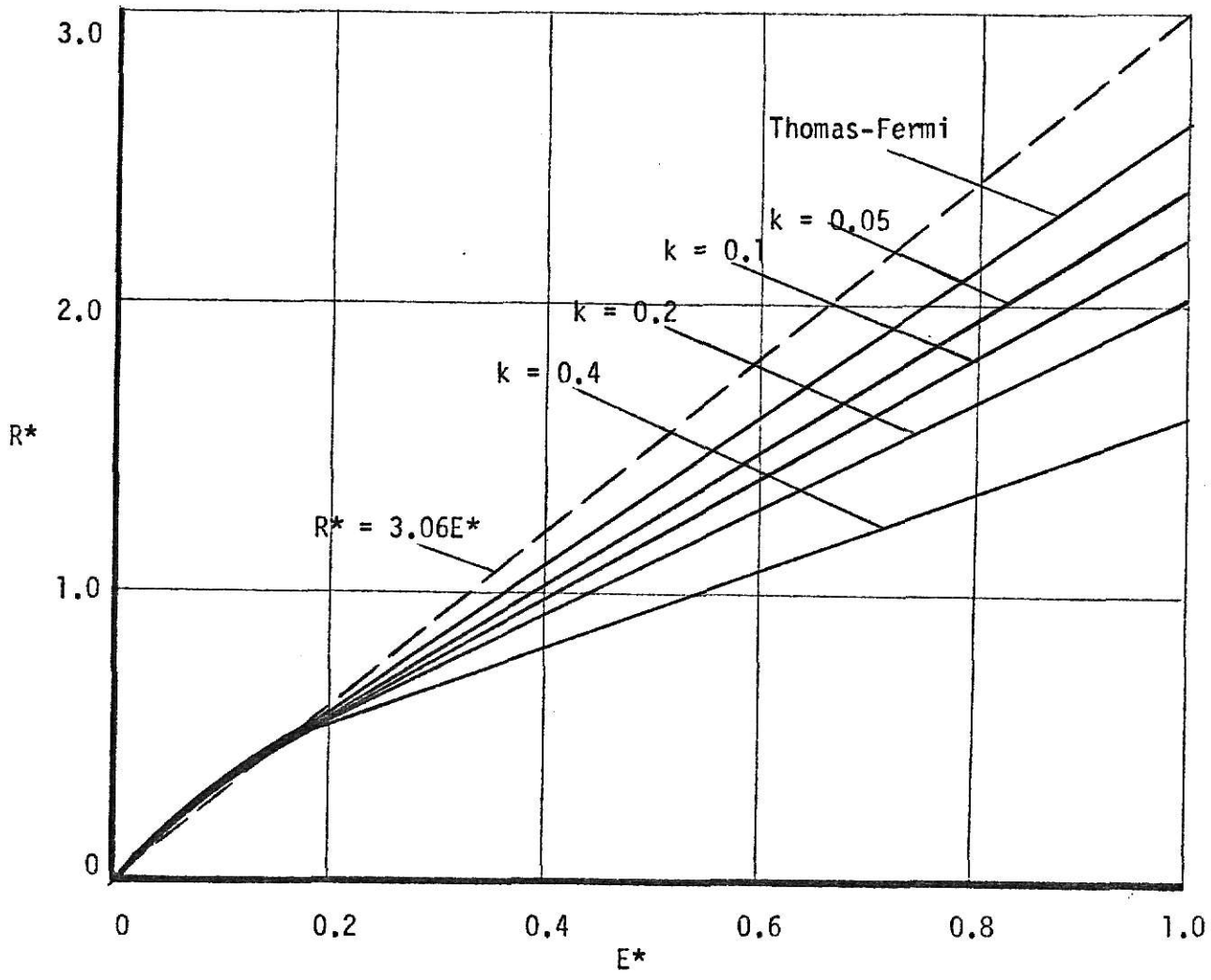

Figure 3-2. Universal range-energy plot. In obtaining Thomas-Fermi curve the effect of electronic stopping has been neglected. Dotted straight line is the standard range, R* = 3.06E*. (After Lindhard et al. Ref. 13.)

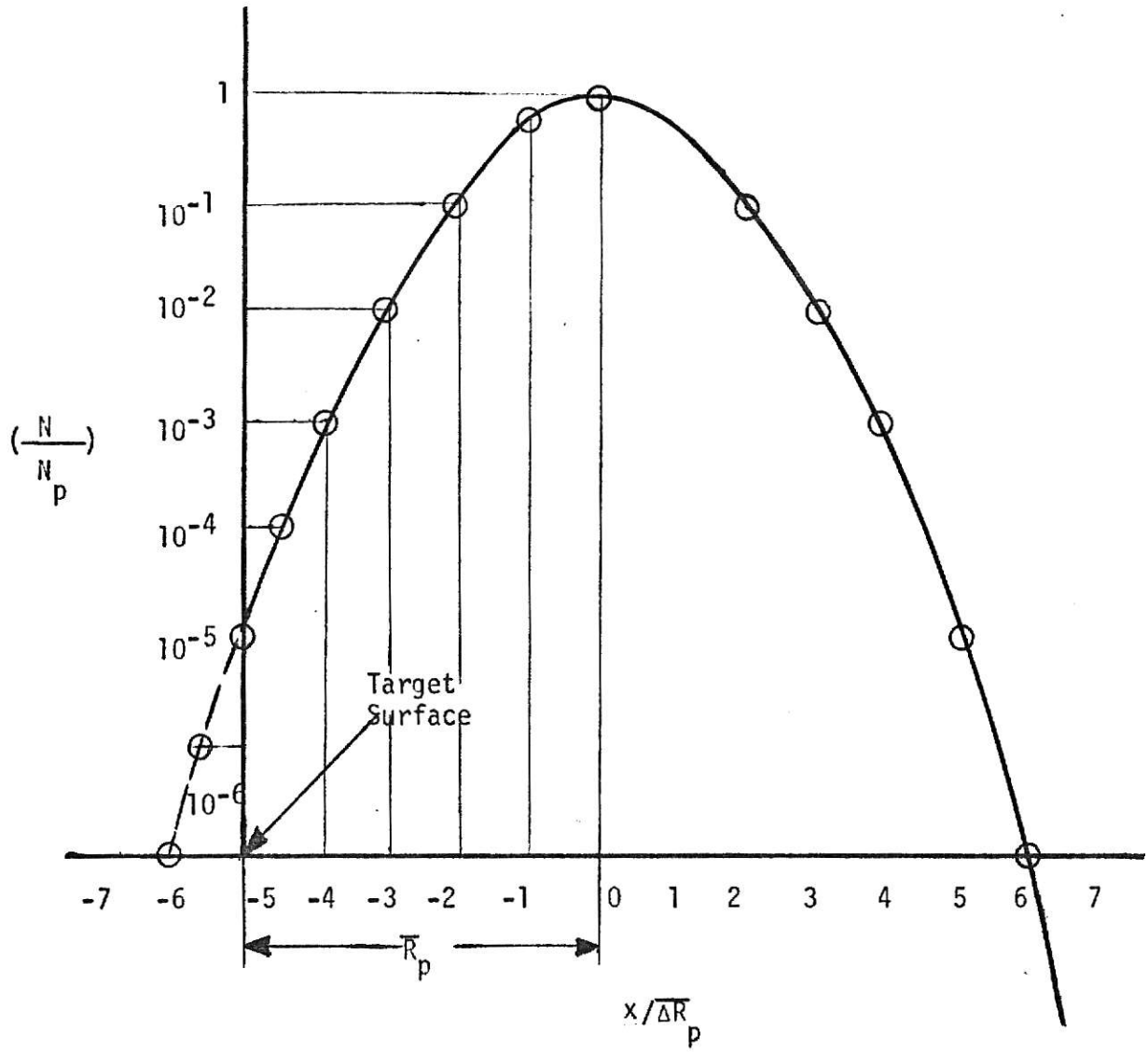

Figure 3-3. Impurity profile for ions implanted into an amorphous target. (After Gibbons Ref. 15.)

species, which will occur at a distance $\overline{R}_p$ beneath the surface of the amorphous target, and has the value[15]

$$N_p = \frac{0.4N}{(\overline{\Delta R}_p)} \tag{17}$$

where N_p is in atoms/cm^3, N in atoms/cm^2, and $\overline{\Delta R}_p$ in cm. On the horizontal coordinate of the Fig. 3-3 the variable x is a function of $\overline{R}_p$ and $(\overline{\Delta R}_p)$. For example, when $x = \overline{R}_p \pm 2(\overline{\Delta R}_p)$ then the ion concentration would drop from its peak value by a decade at this particular level.

A different situation arises when the crystal is precisely oriented along a low-index direction such as <110> or <100>. In this situation if the incident ion follows a path at the center of the channel, then it can never come closer to a target nucleus than about 1 Å, and will therefore lose very little of its energy in nuclear collisions. However, it is very unlikely for a projectile to follow such a path exactly at the center of a channel. Therefore, one possible path that the projectile may follow would be an oscillatory path about the channel axis. This type of motion is called "steering" (i.e., momentum of the projectile is redirected toward the center of the channel), in which the projectile makes successive gentle collisions with the strings of atoms that comprise the walls of the channel[15]. Figure 3-4 is a representation of such an oscillatory trajectory, in which ψ is the angle that the projectile path makes with respect to the channel axis, and d is the distance between atoms in the row. The maximum value that the angle ψ can have before the steering action of the rows of atoms is lost is called the "critical angle for channeling", ψ_c. A computation of ψ_c is given by Gibbons[15]. To prevent the projectile from escaping out of the channel,

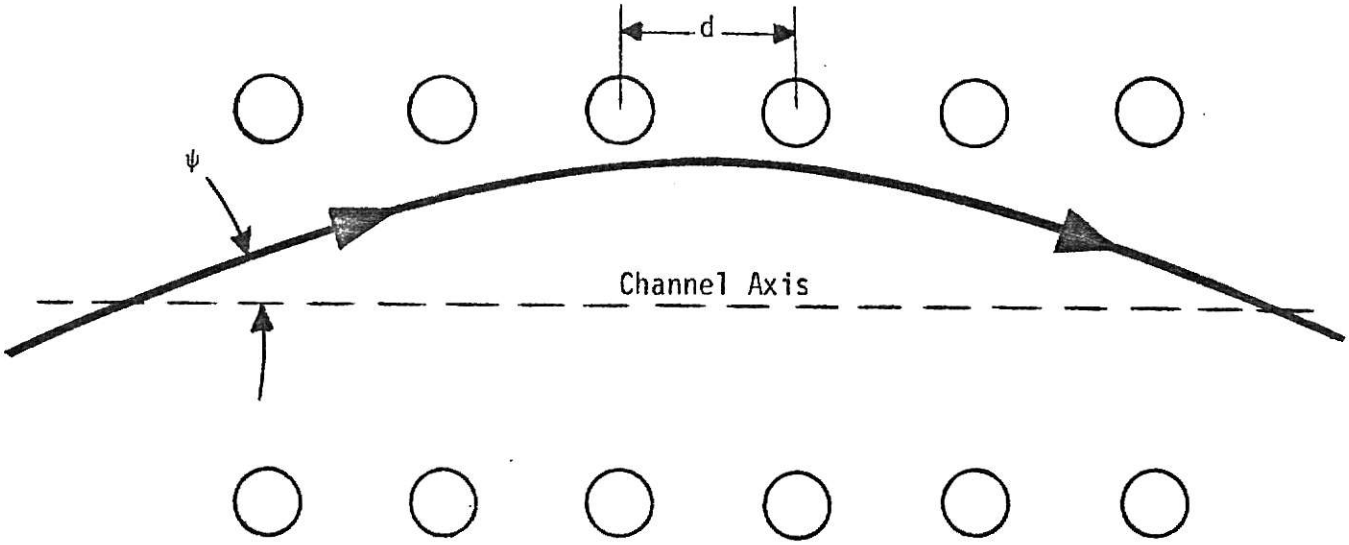

Figure 3-4. Schematic trajectory of a channeled particle. (Realistic value of ψ is $\sim 1^{\circ}$.)

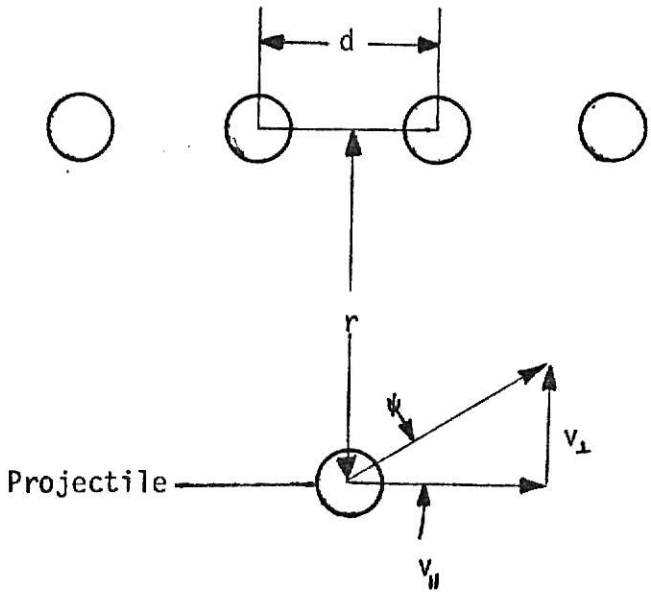

Figure 3-5. Schematic representation for computation of channeling angle.

or to avoid the "wide-angle" scattering that would occur in close collisions of the projectile with the atoms in the row, the following condition must hold

$$r_{min} \geq d \cdot \frac{v_{\perp}}{v_{\parallel}} = d \cdot \tan \psi = d \cdot \psi \qquad (18)$$

where r_{min} is the minimum distance of the projectile from the row of atoms, d is the separation of atoms along the row, $v_{\perp}$ and $v_{\parallel}$ are the perpendicular and parallel velocities of the projectile. The last approximation in Eq. 18 is made assuming ψ to be small. Equation 18 may be defined schematically as is shown in Fig. 3-5.

When an ion beam strikes a crystal surface oriented in a low-index direction (e.g., <110>, or <100>) then the beam can be divided into two parts: a random fraction,and a channeled fraction of the beam. Ion distribution profile of these two beam fractions are obtained separately, since it may be assumed that these two beams are stopped independently of one another. The random beam contains those particles which strike the crystal surface within a distance r_{min} of host atoms. Consequently, these particles are scattered so widely that they are deviated from their initial direction. As a result, the crystal appears to be amorphous for ions in the random beam.

A perfectly "channeled" particle (i.e., one that enters a channel near its center and executes only very minor collisions in its motion down the channel[15]) will encounter a very different stopping environment than will a particle that enters at an angle (comparable to ψ_c) with respect to the channel axis. For these channeled particles the nuclear stopping is less important than electronic stopping, since there exist minor collisions between the projectile and the host atoms.

One important parameter for channeled particles is the "maximum range", R_{max}, which may be obtained from the following formulas

$$(\overline{\Delta R}) \simeq \sqrt{d \cdot R_{max}} \tag{19}$$

or more precisely it may be written as[15]

$$R_{max} = \frac{2E_0^*}{NS_e(E_0^*)} \cdot \left(\frac{E_0}{E_0^*}\right)^{\frac{1}{2}} \tag{20}$$

where in Eq. 19, $\overline{\Delta R}$ is the standard deviation, d is the separation of atoms in the row, and in Eq. 20, E_0^* is a fixed reference energy, E_0 is the initial energy of the projectile, N is the number of incident particles, and $S_e(E_0^*)$ is the electronic stopping which is a function of E_0^*.

In this chapter basic principles, theoretical approaches, and some structural complications which might arise during the process of ion implantation have been discussed. Later, in the chapter on experimental results and discussion, one very important respect of ion implantation, namely, radiation and structural damage, will be discussed.

CHAPTER IV

ION IMPLANTATION APPARATUS

4.1 Introduction

In the previous chapter the theoretical basis of ion implantation was discussed; thus we are now in a better position to discuss the type of equipment necessary for implantation of various ion species into different substrates at different energy levels. We will first discuss the basic equipment necessary for ion implantation, and then describe some of the practical arrangements which have been used. Finally, the latter part of this chapter will illustrate the experimental set up that has been used by the author to attempt to "form" p-n junctions.

4.2 Ion Implantation Systems

The basic requirements for an ion implantation system, shown in block diagram form in Fig. 4-1, comprise the following sections:

(i) Ion Source

(ii) Extraction and pre-focusing of ion beam

(iii)Acceleration tube

(iv) Mass analyzer

(v) Final focusing of ion beam

(vi) Beam sweeping system

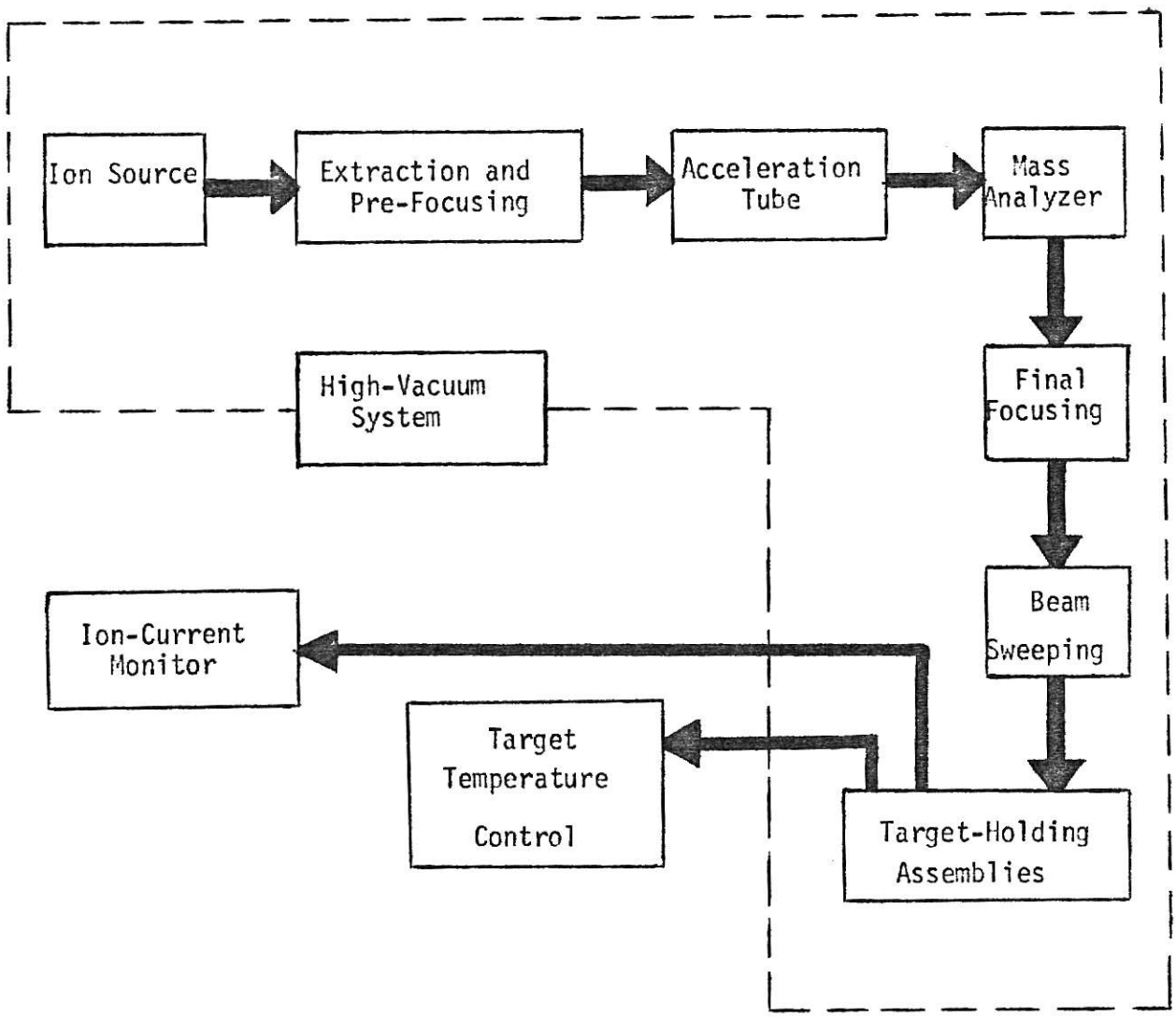

Figure 4-1. Block diagram of ion implantation system.

(vii) Target-holding assemblies

(viii)High-vacuum system

(ix) Target temperature control

(x) Ion-current monitoring system.

An operational system is shown for moderate implantation energies in Fig. 4-2. In this figure some additional deflection plates are shown, which are used for further alignment of the beam.

Limitations in equipment put accelerating voltages into 3 ranges; low, medium, and high. These 3 ranges of energies are sometimes catagorized into the following: low energies 0-25 KeV, medium energies 25-100 KeV, and high energies greater than 100 KeV. High voltages for implantation are usually supplied by Van de Graaff generators and this necessitates that the target be operated at ground potential.

In the following sections the experimental apparatus used by the author will be briefly described and discussed.

4.3 Experimental Apparatus

The complete system consisted of three elements of cylindrical symmetry placed in a horizontal linear array: (i) the Colutron ion source; (ii) an electrostatic focussing lens set of three steel cylinders; and (iii) a shuttered specimen target assembly incorporating a beam current monitor (Faraday cup). The whole array was placed along the horizontal axis of a Pyrex glass "cross" chamber mounted on a Varian VE 20 vacuum unit capable of attaining 1×10^{-6} torr without liquid nitrogen cooling. A schematic representation of this system is shown in Fig. 4-3. In the following subsections the experimental system components will be discussed.

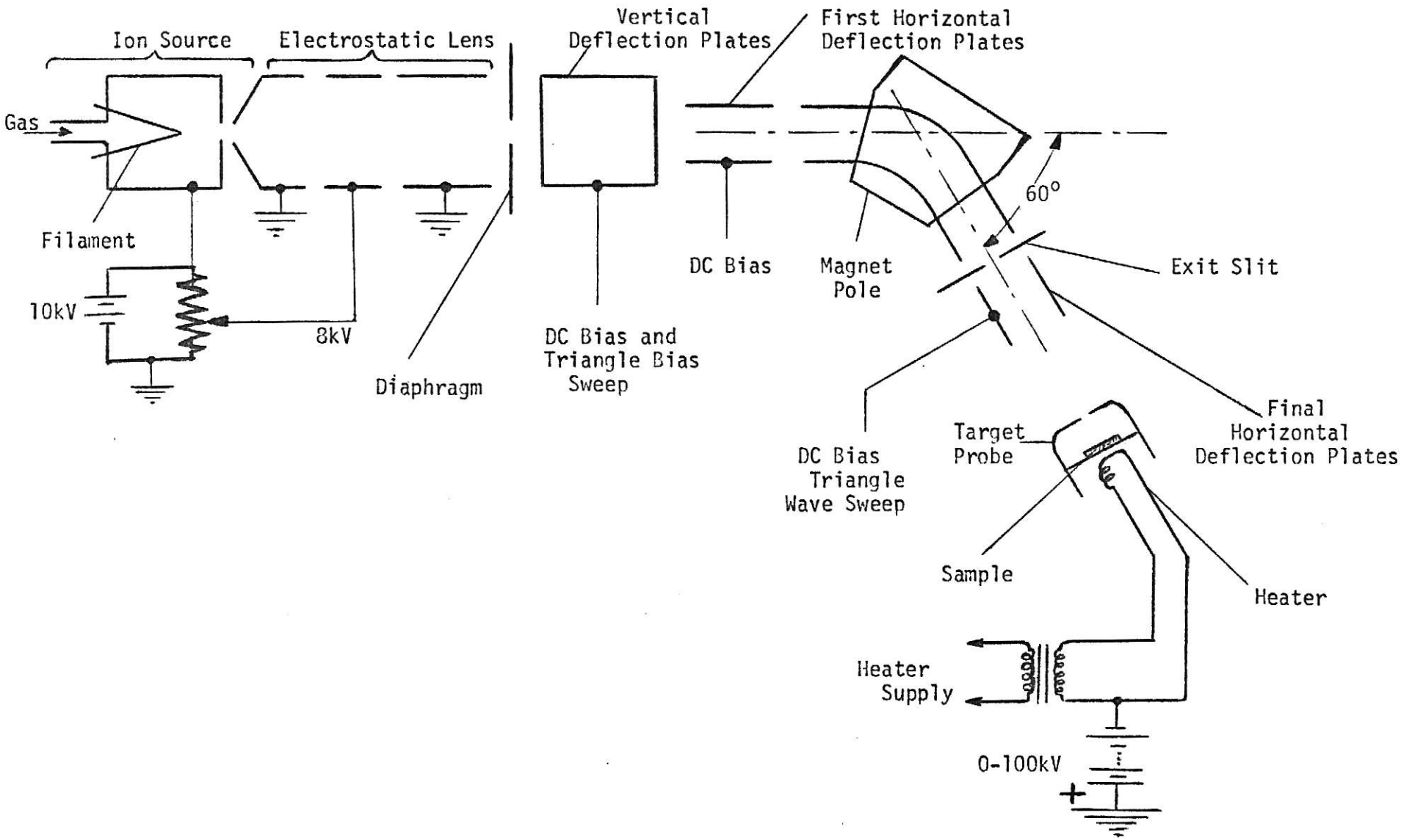

Figure 4-2. System of ion implantation with mass analyzing magnet for ions of moderate energies. (From Gibbons, 1968)

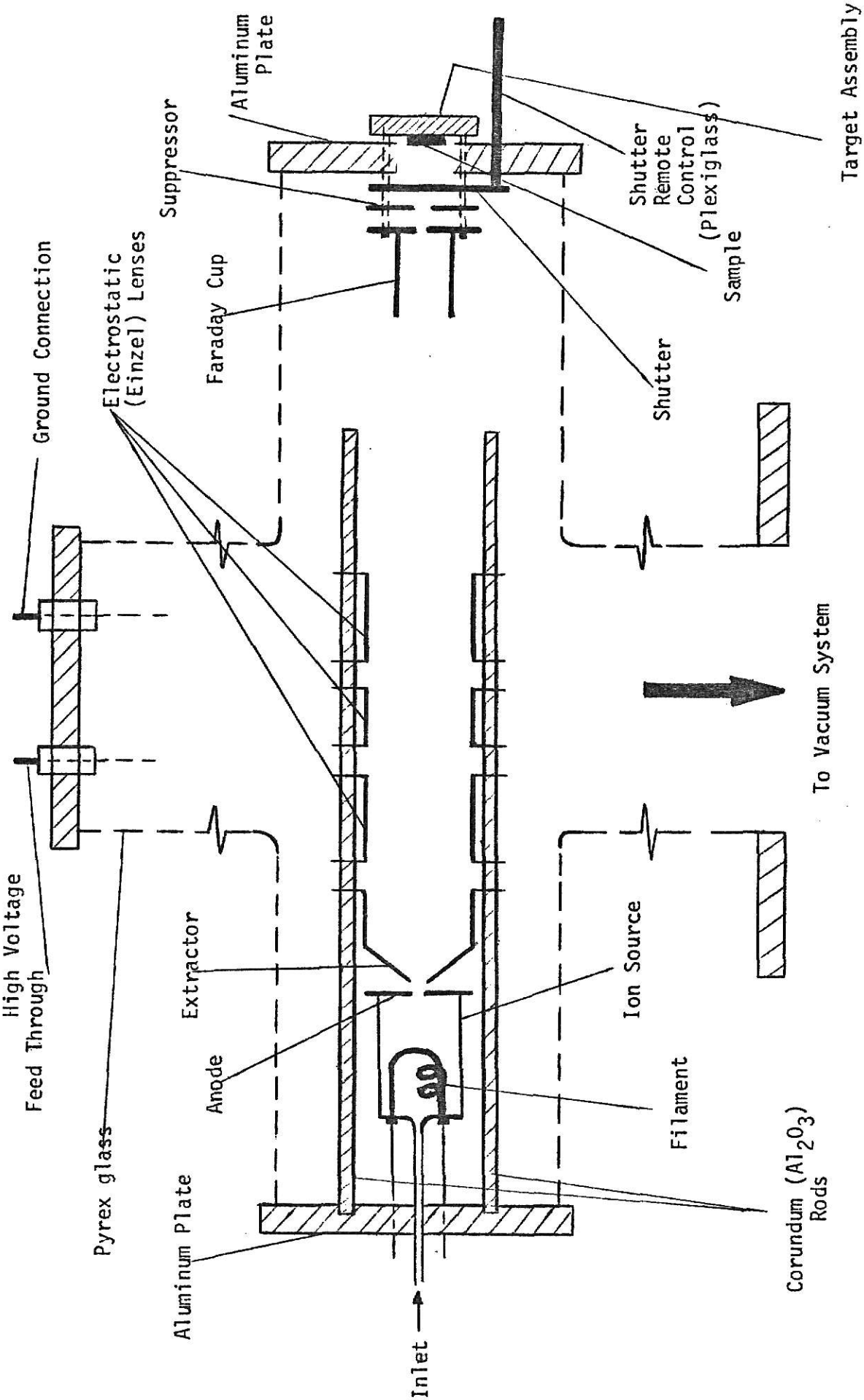

Figure 4-3. Experimental ion implantation system. (Used for low energy implantations ($\lesssim$ 25 KeV).)

4.3.1 Ion Source

The ion source is perhaps the most critical component of an ion implantation system. There are mainly four different types of ion source, as listed below

(i) Surface ionization source

(ii) RF ion source

(iii)Magnetic oscillating electron source

(iv) Sputtering ion source

the detailed description of these four ion sources are given by Large (1969).

The source used in the present experiments, was a cylindrically symmetrical chamber, 1.8" long and 1" in diameter machined out of boron nitride ceramic. A threaded stainless steel tube ¼" in diameter screwed into the back end of the chamber and acted as feed pipe for the gas to be ionized. The front end was closed by an annular cap of boron nitride, which held over the end of the chamber a 0.020" molybdenum sheet disc, pierced with a 0.020" diameter central hole. This disc was the source anode. The filament was made of tungsten wire (guage 0.015") wound into a slighly tapered spiral and attached to molybdenum leads by means of tightly wound spirals at the filament ends. In operation a d.c. arc discharge was confined to a small volume between the filament and the anode by a boron nitride shaped insert placed in front of the filament and behind the anode. A cross-sectional view of this ion source is shown in Fig. 4-4.

4.3.2 Electrostatic Lens System

The beam area and the beam density depend upon the type of focusing which is used with the ion source and the distance between the source and the target. One method for increasing the versatility of the ion source is

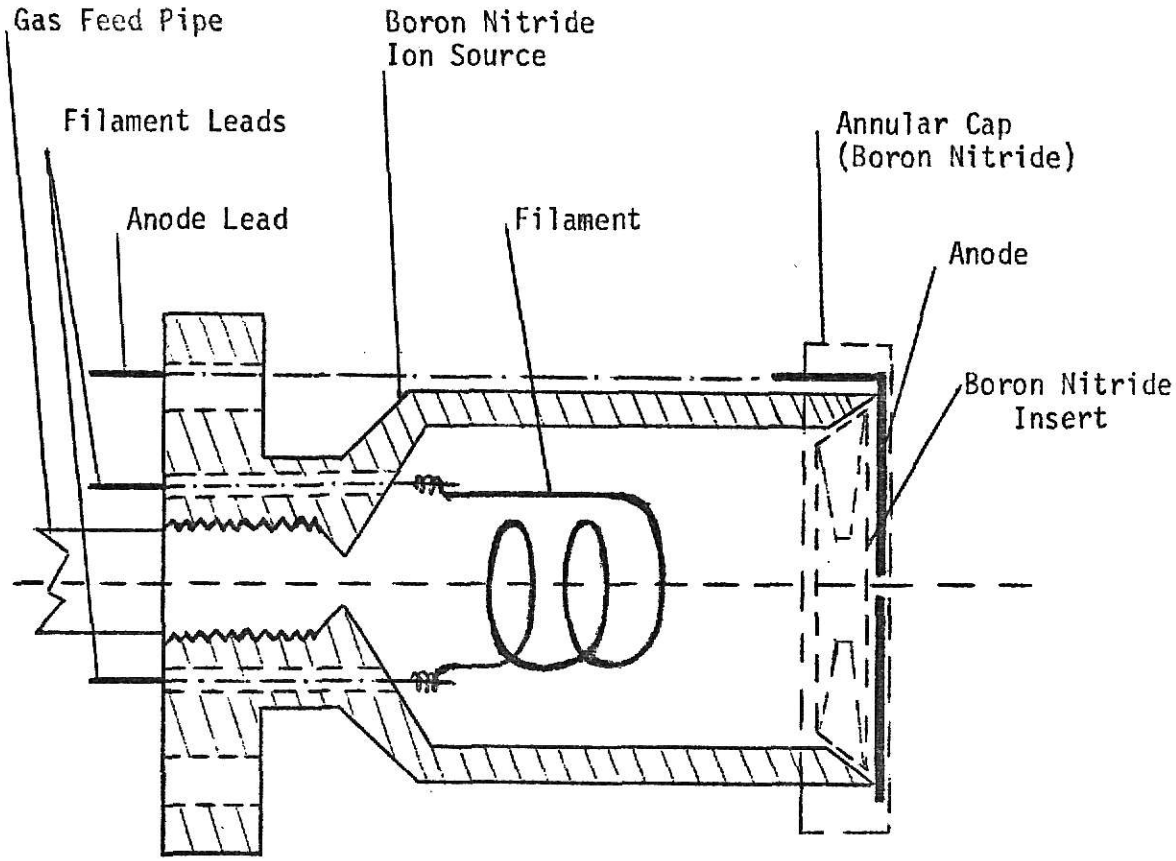

Figure 4-4. Cross-sectional view of the ion source used in the experiments.

to use an Einzel lens (equipotential lens). This type of lens uses three electrodes, two of which are at ground potential. The focal properties of this lens are due to the radial forces arising from the shaped electric field in the lens. A cross section of an Einzel lens is schematically illustrated in Fig. 4-5. Equipotentials of the electric field are shown in this figure along with the force vectors associated with them.

A series combination of "deceleration-acceleration" and"acceleration-deceleration" gives the strongest focusing effect over short distances. One point to be noted in this type of lens is that the effect of the lens depends upon the changing velocities of the beam in the field region. The strongest focusing effects occur in regions B and C (see Fig. 4-5), since the beam is traveling relatively slowly at these regions. The effects in the A and D regions are less because of the higher particle velocities.

In the experimental set up, the original array consisted of three cylinders of steel, diameter 1.6", mounted in aluminum rings. One cylinder length 1.2" was capped with 120° cone containing a 3/16" axial hole, while the other two were right cylinders of length 2.0" and 1.2". It was decided, after some preliminary experiments, to use the conically ended cylinder as an extraction electrode next to the ion source, and a further 2.0" length cylinder was made, so that three cylinders could then be grouped after the extractor electrode to form a focussing lens array. To overcome the heating problem, the four cylinders were mounted on three corundum (Al_2O_3 ceramic) rods passing through holes in the aluminum rings to form an adjustable "optical bench" arrangement, since the focal length of the lens array is critically dependent on the spacings or "gaps" between the cylinder sections. The final lens arrangement is illustrated in Fig. 4-6.

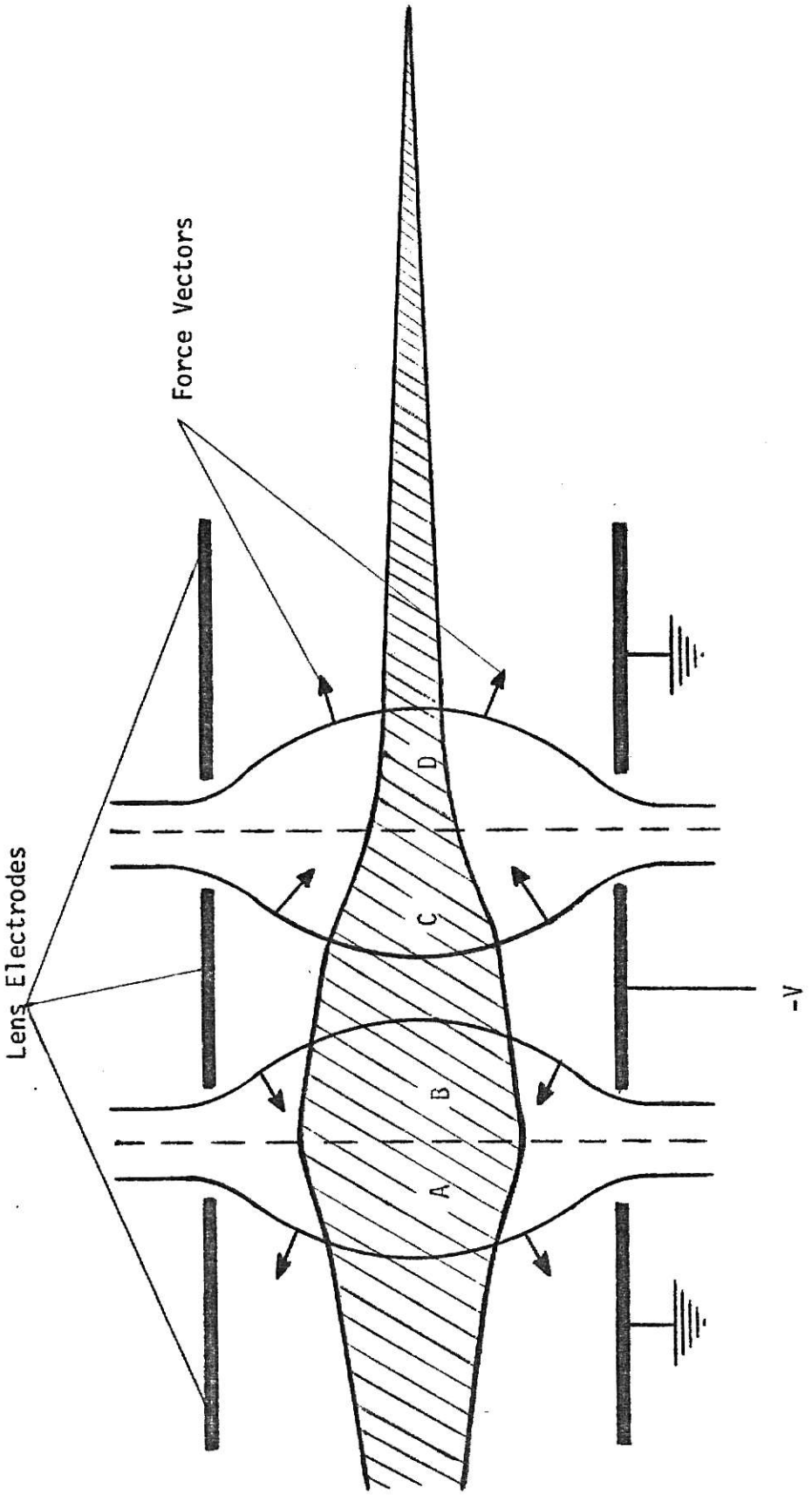

Figure 4-5. Schematic representation of an Einzel lens with potentials and associated force vectors.

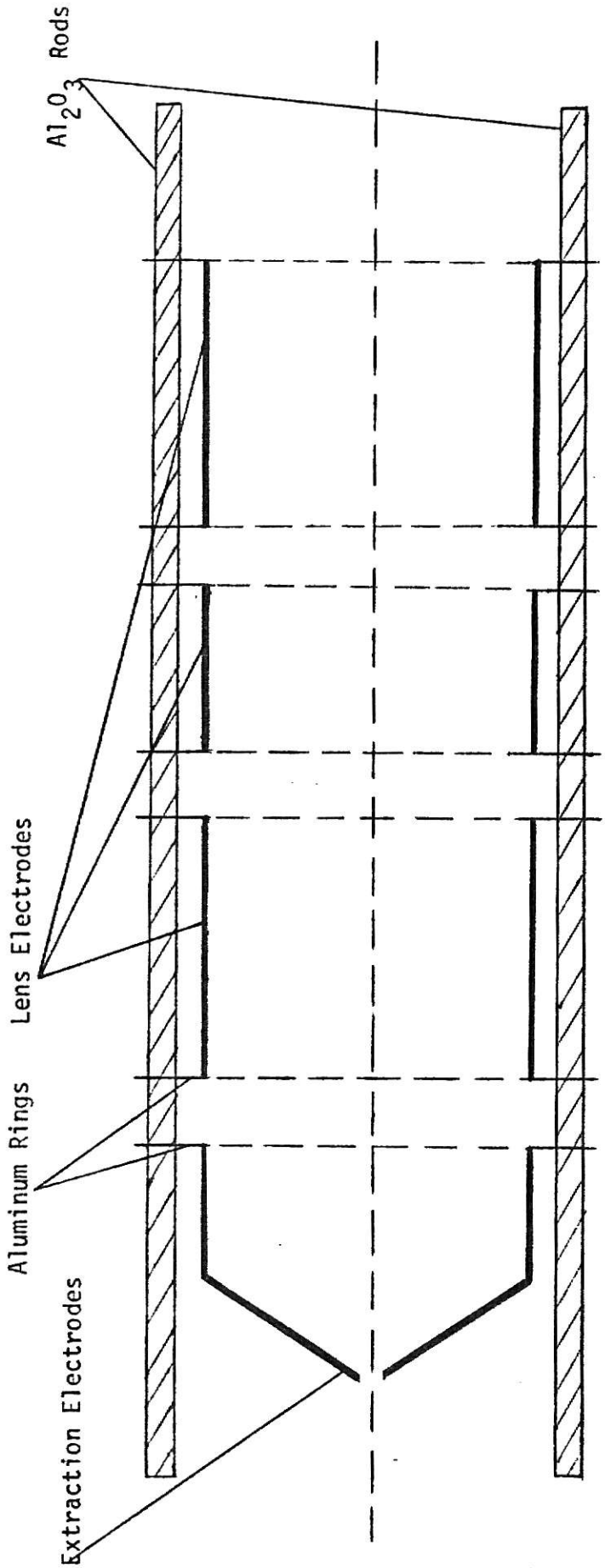

Figure 4-6. Final experimental arrangement of lens and extraction electrodes.

The potential required to operate such a lens is roughly equal to the incoming beam energy, which was acquired through the extraction electrode. Therefore, the resulting addition of energy to the beam is zero, making it possible for one to vary the beam area and current density without altering the particle energies. When just an ion source is used a beam area of less than a few cm^2 is difficult to obtain. However, using an Einzel lens it is practical to work with beam areas of 3 to 4 mm^2. As a result, high current densities can be obtained. In an Einzel lens system the beam characteristics can vary and have three different configurations. These characteristics, focused beam, collimated beam, and divergent beam, are shown in Fig. 4-7. These variations can result from changing the spacings between the cylinder sections, or by altering the voltage ratio among the lens electrodes.

4.3.3 Target Assemblies

After emerging from the final section of the lens array the ion beam was passed first into a Faraday cup, a steel cylinder 3.25" long and 1.6" diameter, open at the incident end and containing a 3/16" aperture in a steel plate closing the far end. Behind this, and insulated from it, was a secondary electron suppressor plate containing a ½" diameter aperture. A steel plate shutter, also insulated from the other components, could be rotated into a position behind the suppressor plate. In various experiments, to be described in the next chapter, this shutter was used to hold the specimen to be implanted.

In the experiments, before the actual implantation would take place, it was necessary to know the beam configuration. Thus, a plexiglass disc covered with zinc sulfide fluorescent powder on the top of a thin smear of silicone vacuum grease was positioned in place of the specimen holder. The ion beam image could thus be observed from outside the vacuum system. This screen

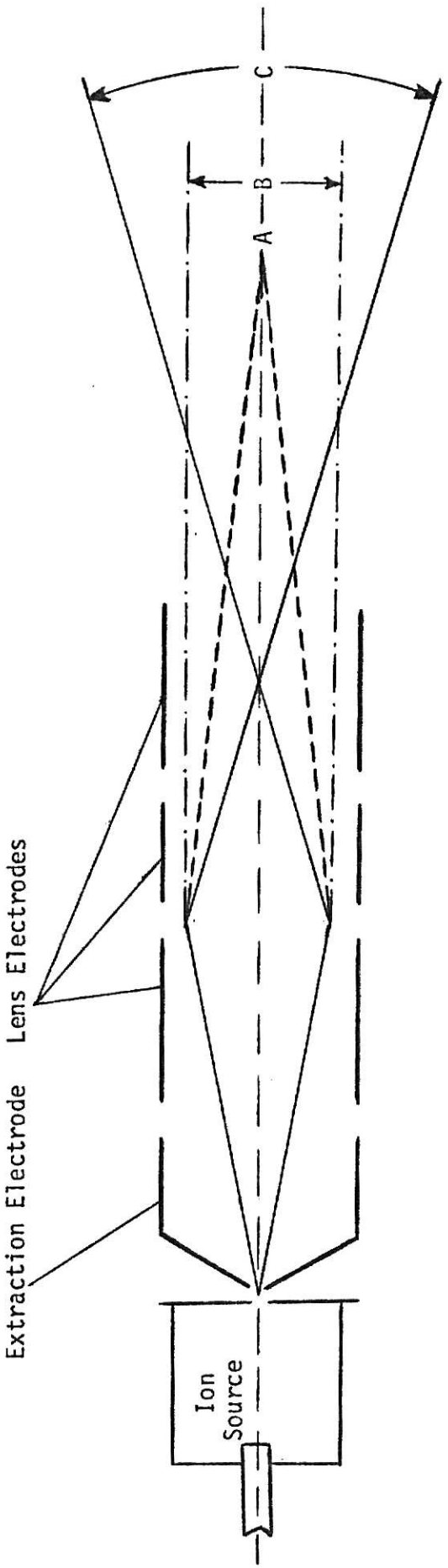

Figure 4-7. Possible beam configurations. (A) focused beam. (B) collimated beam. (C) divergent beam.

(plexiglass disc) was subsequently modified by painting a small central silver-dag disc connected by a thin silver-dag strip to the edge of the screen so that the ion current at the center of the screen could be measured.

In the following chapter the operation of this system along with the obtained and measured results will be discussed.

CHAPTER V

OPERATIONS AND RESULTS

5.1 Introduction

This chapter is basically divided into two parts. The first part includes a discussion and description of operations involving the experimental system along with an investigation of the performance of a commercial ion source for future use in a high energy Cockcroft-Walton accelerator (the Colutron positive ion source). The second part is a description of ion implantation experiments, followed by results of resistivity measurements. Finally a review of possible structural damage to target materials after implantation is given.

5.2 Operations of the Experimental System

The experimental set up which was used by the author (see Fig. 4-3) comprised basically the following sections: ion source, electrostatic lens array, and target assemblies. The first part of the experiments which investigated the performance of the commercial ion source also included the arrangement of the electrostatic lens electrodes for the best focusing (determination of the proper "gap" size between electrodes), and the target assemblies. In the following subsections operations of these components along with operations of some other related parts will be described and discussed.

5.2.1 Operation of Ion Source

After several runs the inside of the ion source became coated with a black powder (probably tungsten oxide). This necessitated dismantling and cleaning the interior of the source, and inevitably meant replacing the tungsten filament which had become brittle due to grain growth. The operation described here assumes that a new filament and newly cleaned (and hence not outgassed) source are being used. The chamber was pumped down to $\sim 1 \times 10^{-6}$ torr and the D.C. filament source turned on to pass $\sim$ 5 amps (at 15 volts). Soon the pressure rose to $\sim 10^{-4}$ torr as the system warmed up and outgassed, and then slowly fell to its original value. The current was then increased to 8-10 amps and the whole process repeated until the filament could be run at $\sim$ 15-18 amps without pressure change. This took 30-60 minutes.

Next, with the filament at 10-12 amps the anode bias was set at + 100 V, and the gas to be ionized slowly leaked in through a needle valve. The striking of the arc was detected by firstly, an arc current of $\sim$ 0.5-1.0 amps (between anode and filament) and secondly, a bright glow at the anode end of the ion source (whitish for nitrogen, bright red for argon, pink for helium). The gas flow could then be reduced slightly, without loss of current. After some minutes operation the glow at the anode end spread along the length of the source, as the entire tube became heated. Typical characteristics are shown in Fig. 5-1.

After each set of runs the outside of the source showed superficial cracks which could be removed with a mild abrasive cleaning powder. Also, sometimes after the runs there were small "glass" like bubbles on the surface of the source which could be removed in a similar manner. These bubbles could have possibly resulted from some complex chemical reactions at the

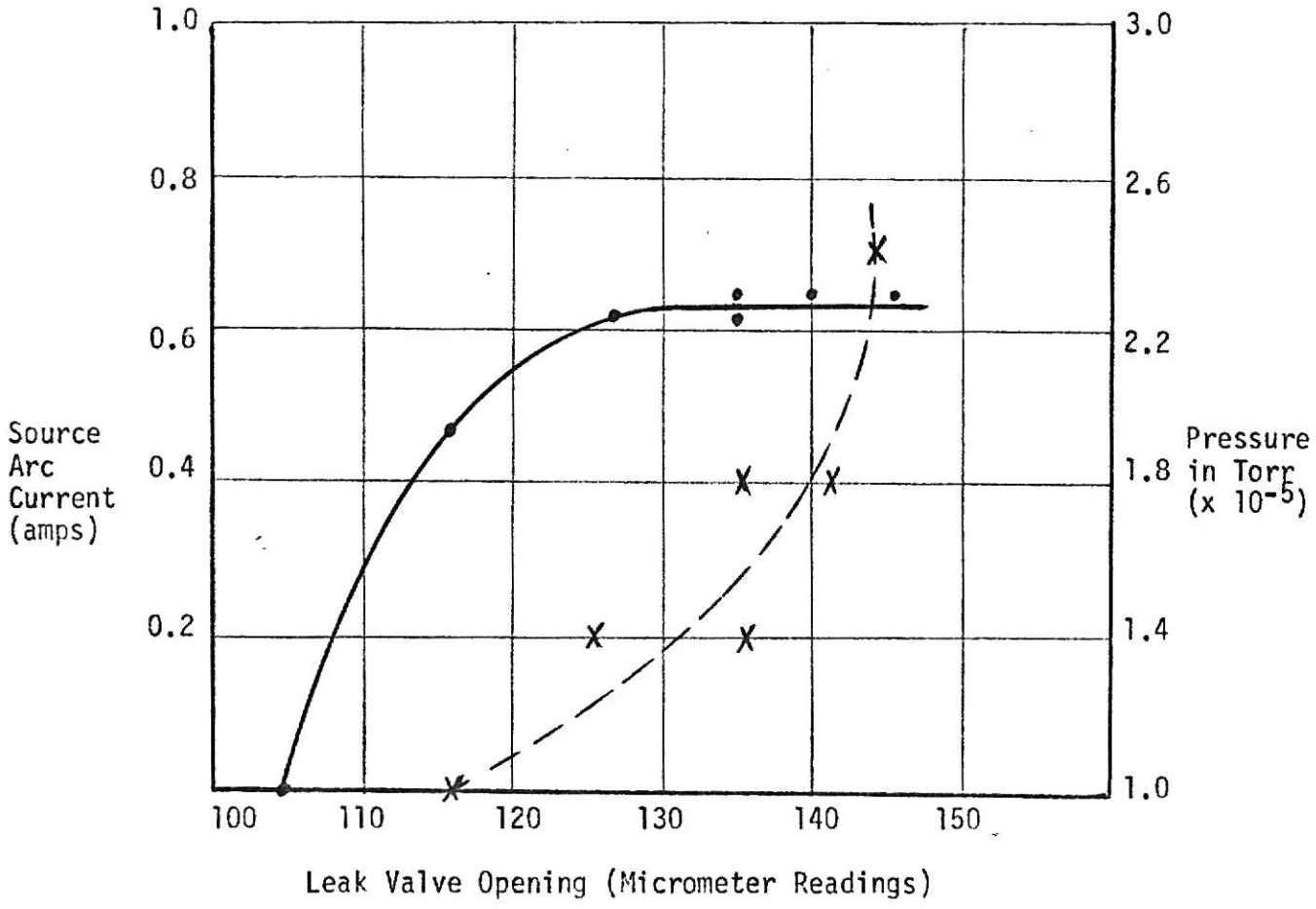

Figure 5-1. Typical characteristics of the ion source arc current and the pressure of the chamber versus the leak valve opening. (Full-drawn curve is the source arc current vs. leak valve opening, and dashed-like curve is the pressure vs. leak valve opening.) (Anode bias 70 V, filament current 13.8 amps.)

extremely high temperature on the surface of boron nitride source. The cleaning of the source created a problem. The boron nitride with its "clay" like character could be washed-out easily, and so the source slowly changed its wall thickness.

5.2.2 Filament Lifetime

Three relatively unreactive gases have been used - helium, nitrogen, and argon. The filament lifetimes, in a rather sparse number of experiments, appear to be independent of the gas being ionized. The lifetime is in excess of 20 hours but probably less than 30 hours, for a 0.015" tungsten filament run at $\sim$ 12-14 amps and bias of $\sim$ 60-100 V. (i.e., an arc current of 0.5-1.0 amps.)

5.2.3 Adjustment of Electrostatic Lens Array

The unipotential or Einzel lens arrangement consists of three cylinders, usually of equal diameter (2R) but with the middle section of a different length (L_i/R: it is convenient to give all dimensions as a ratio to the tube radius R) than the outer two sections (see Fig. 4-5). Electrostatic equal potentials V_o are applied to the outer electrodes and a different potential V_i to the middle section L_i. The focal length is dependent on L_i, V_i/V_o, and the lens gap spacing which practically has a lower limit set by breakdown between the middle and outer cylinders.

The present arrangement was a modified version of the above description (see Fig. 4-6). The 120^o capped cylinder was placed close (0.125") to the anode, with a variable extraction voltage usually $\sim$ 1-2 KV applied to it, so that field penetration through the anode aperture was obtained and positive ions could be extracted. The three lens sections were spaced 0.125" apart (see below), the middle section being the shorter cylinder. The two longer

outer cylinders were connected together at a variable voltage ∿ 10 KV and the central section was connected to the extraction electrode. These values were arrived at partly by experimental trial and error and partly by using data of Klemperer[16] and Liebmann[17].

5.2.4 Target Arrangement

The Faraday cup, secondary electron suppressor, shutter and (if used) screen were all connected independently to a -10 KV source via microammeters, so that the ion beam current could be monitored at various stages in its transit through the target system. Initial experiments also used a phospher screen (fluorescent powder on an aluminum foil annular disc) placed around the outside of the Faraday cup and quickly showed that under incorrect conditions of lens arrangement a widely diverging beam was formed. When correct settings were achieved the beam was confined to a cylindrical volume coaxial with the Faraday cup axis and of small diameter. One critical adjustment here was the centering of the anode aperture on the axis of the system. (Ideally, this should be a micrometer adjustment manipulated from outside the vacuum system.)

If the beam is produced as a narrow axial pencil with small divergence it should all pass through the 5/32" hole at the end of the Faraday cup and hit the shutter, target, or screen without producing any current at the cup. A measure of the efficiency of the lens system in achieving this ideal configuration can be determined from the ratio of ion current at the shutter to the total collected ion current. Total ion current will be that measured at the Faraday cup and the target (or shutter) added together. The variation of this ratio (expressed as a percentage) is given in the graph of Fig. 5-2 as a function of the voltage on the outer sections of the lens array. A constant

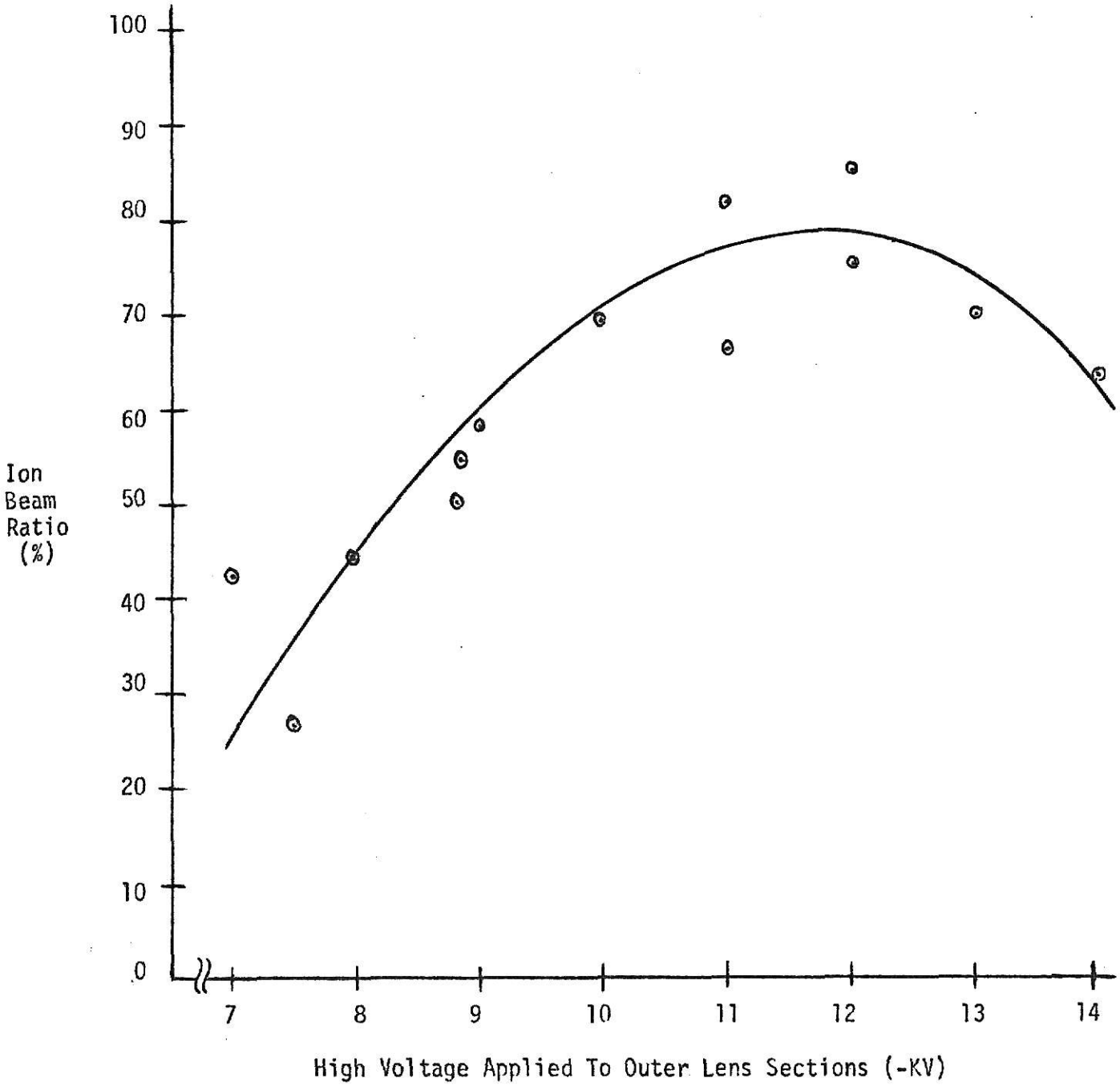

Figure 5-2. Ratio of total ion current to current at the shutter versus the applied voltage to the lens sections.

voltage of -1.6 KV was applied to the extraction electrode and the middle section of the lens system, and all sections were spaced at 0.125". It can be seen that efficiencies of 75-85% are being achieved.

5.2.5 Stability of Ion Source and Focussing Array

The system gave steady ion beams over considerable periods (45 minutes) provided that the ceramic Al_2O_3 support rods (see Fig. 4-6) were carefully cleaned of all aluminum tracks (which could be produced when the lens sections were slid into their correctly spaced positions along the rods) and provided the lens gaps and applied voltages were adjusted to correct values to prevent breakdown. A gap of 0.125" would tolerate a potential difference of $\sim$ 14 KV before arcing occurred. Toward the end of a filament's lifetime the current needed to produce a particular ion current fell slowly presumably because the filament diameter was being reduced by oxidation of tungsten to volatile tungsten oxide.

5.3 Implantation Experiments

Alkali halides are a convenient class of materials to use as experimental targets, because when subjected to many types of irradiation (e.g., X-rays, or electron bombardment) they become colored. The color produced depends on the particular alkali halide, and is due to the production of so called F centers by the irradiation. The F center defect then has been identified by electron spin resonance studies as an electron trapped at a negative ion vacancy, and in sodium chloride gives an absorption band at $\sim$ 5000 $\mathring{A}$ wavelength.

It was decided to try the effects of low energy positive ion bombardment on freshly cleaved rock salt samples, in the hope that optical examination of

the colored area would give at least a qualitative indication of the beam area.

In later experiments p-type silicon slices were implanted in an attempt to "form" p-n junctions.

5.3.1 Implantation into Sodium Chloride

Figure 5-3 is an illustration of the results of some preliminary argon ion bombardment experiments on rock salt crystal surfaces. Part (A) of this figure is a low magnification micrograph showing the radiation damage as apparent clusters of black spots or dark gray regions. In the (B) part of this micrograph, at higher magnification, the bombarded areas are shown to exhibit considerable complexity of surface structure.

The most interesting result was obtained by bombarding a freshly cleaved (001) surface with 3 μA of nitrogen ions accelerated to 6.9 KV for 14 minutes. A dark brown patch ∿ 3 mms. diameter was visible after bombarding the rock salt. The total ion dose corresponds to ∿ 3×10^{17} ions cm^{-2}. The colored patch disappeared within 24 hours and no effects were visible in the bombarded region under low power examination. Seven days later some small spherical voids ("bubbles") could be seen under low power magnification within the crystal beneath the bombarded surface. Several days later two large bubbles about 1-2 mms. diameter could be seen by the unaided eye, and low power examination revealed that they were composed of myriads of smaller bubbles clustered together.

It would appear that the implanted nitrogen initially produced color centers which were annealed out fairly rapidly at room temperature, possibly converting nitrogen ions to nitrogen molecules. The gas molecules then migrated together by a slower room temperature diffusion process, eventually forming macro-bubbles within the sodium chloride crystal.

Figure 5-3. Surface damage as a result of argon ion bombardment on rock salt crystal. (A) low magnification. (B) high magnification.

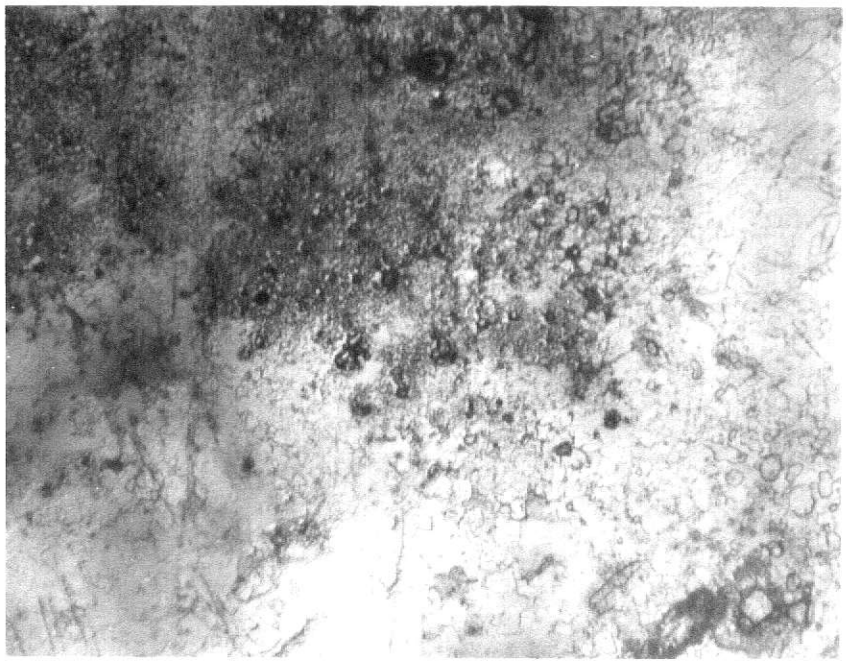

(∿ x 25)

(A)

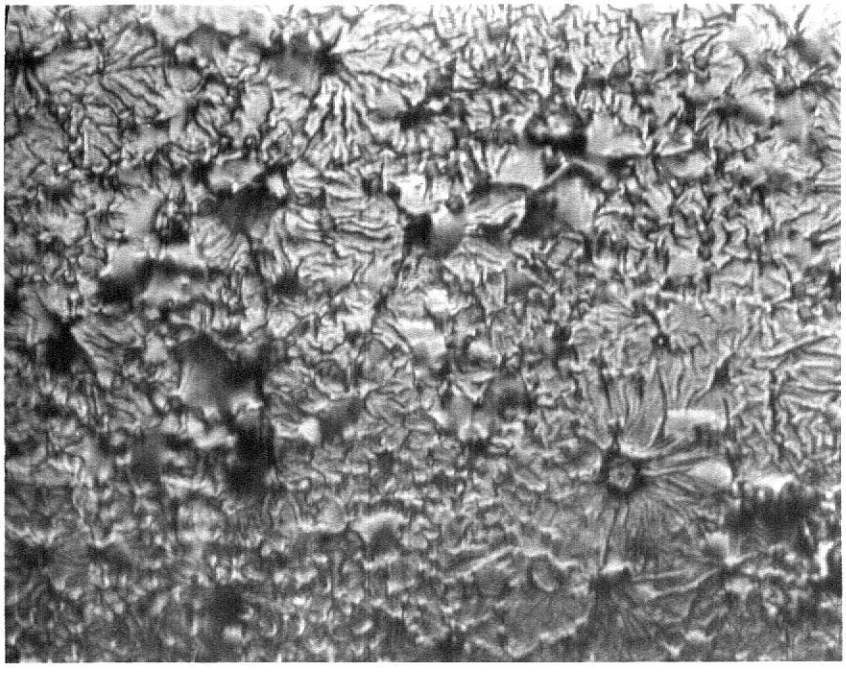

(∿ x 150)

(B)

Figures 5-4 are taken from this nitrogen bombarded rock salt crystal after 8 months of clean air annealing. The "bubble" formation is clearly shown in Fig. 5-4 (A) with magnification of about 40 times, in which there are now 3 bubbles of different sizes. Figure 5-4 (B), which is the bubble at the upper left hand corner of Fig. 5-4 (A) magnified about 60 times of its actual size, shows cubic structures in which clusters of bubbles are shown. High magnification micrographs are shown in Figs. 5-4 (C) and (D). Another interesting point which can be observed, besides the formation of bubbles inside cubical structures, is a frequent appearance of "double bubbles" inside a cube. This is shown by an arrow on Fig. 5-4 (D). It appears that one bubble has been formed inside a second one and both appear to be enclosed within a cubical void. One may conclude an explanation for this bubble formation as resulting from migration of implanted ions to form gas molecules which in turn migrate further to form gas bubbles. If two sets of these migrations take place simultaneously in one region then the double bubble formation occurs. The cubic voids may result from agglomeration of vacancies caused by the ion implantation damage, but this can only be a tentative explanation without further experiments. It is planned to pursue these studies further, using controlled annealing procedures to observe the changes in bubble and void occurrence.

5.3.2 Implantation Into Silicon

A series of experiments involving the implantation of nitrogen ions into p-type silicon material were carried out in attempt to "form" p-n junctions. Silicon slices of 0.020" thickness and 1.0" diameter were glued to the shutter plate and bombarded with various nitrogen ion density beams. Due to lack of a beam sweeping arrangement in the experimental ion implantation system the

Figure 5-4. Nitrogen ion bombarded rock salt crystal showing the "bubble" formation. (A) low magnification showing the 3 bubbles. (B) higher magnification of the largest bubble in which the cubical orientation at the edge of the bubble is shown.

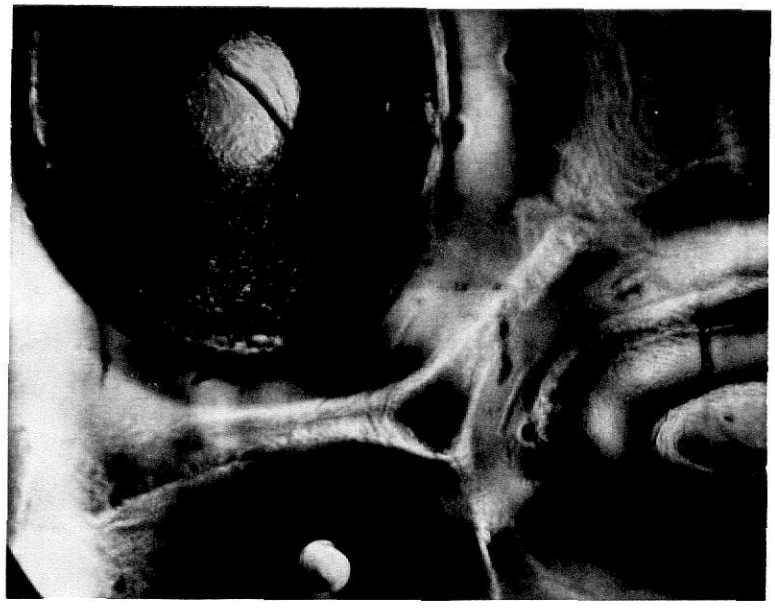

(~ x 40)

(A)

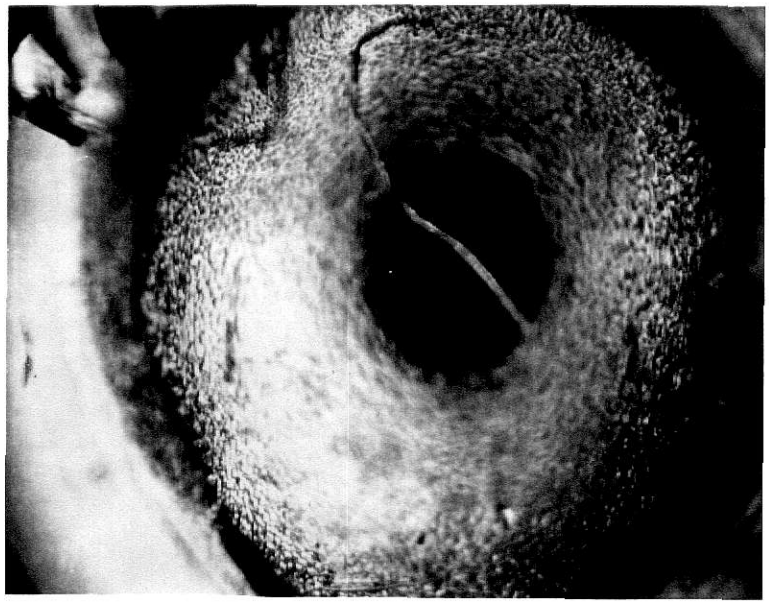

(~ x 60)

(B)

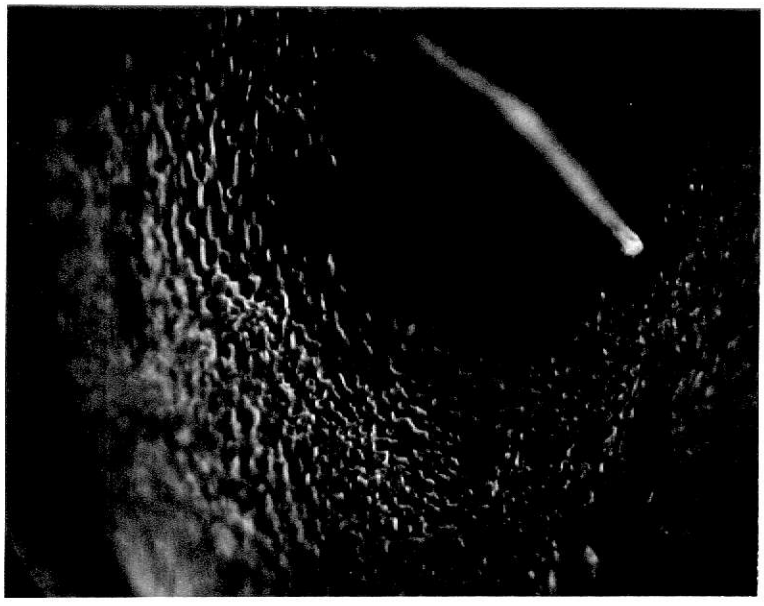

(∿ x 100)

(C)

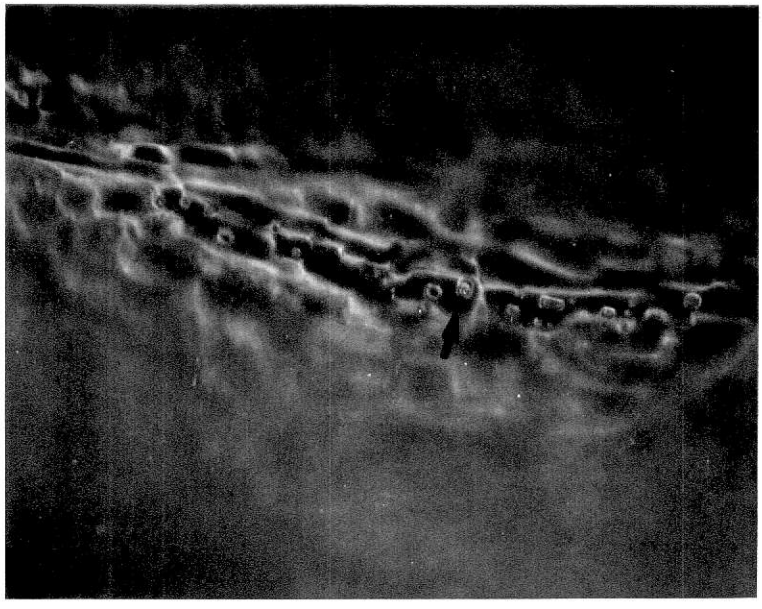

(∿ x 200)

(D)

specimen was moved instead. Oscillation of the shutter (with the silicon slice glued to it) allowed an arced track $\sim$ 3 mms. wide and $\sim$ 3 cms. long to be produced. In other experiments the shutter was moved in steps to produce a set of discrete bombarded circular areas on the silicon disc.

In all cases the bombarded regions appeared to be coated with a brown deposit. A few seconds immersion in 40% HF (hydrofluoric acid, which does not interact with silicon) removed the coating from the central portion of the patch or track, leaving bright clear areas, but at the edges the brown discoloration remained, even with prolonged immersion in the acid.

It is probable that the brown coating is due to contamination similar to that produced on electron microscope apertures and specimens. This is due to polymerization of residual long chain hydrocarbons in the vacuum system by electron bombardment, which produces cross-linkage and hence an adherent carbonaceous film. The cure for prevention of contamination is either to work in a lower pressure vacuum system, or to use heated bombarded areas, so allowing the absorbed molecules to reevaporate.

In order to produce a set of p-n junctions it is necessary to mask areas of the p-type silicon from the ion beam. This can be achieved by vacuum deposition (through a suitable mask) of a heavy metal on the surface of the wafer to be bombarded. In the experiments carried out by the author a gold (Au) layer of a few hundred $\mathring{A}$ thickness was used. This had the additional advantage of providing another material for study of the effects of the ion implantation.

5.4 Resistivity Measurements

A four-point probe resistivity measuring apparatus has been used to reveal changes in the conductivity in the bombarded regions. Results of measurements on the silicon samples indicated resistivity changes. But, most of these results were not too meaningful because of the fact that the results of measurements depended on the geometry of the samples, and also in which region of the sample the measurements were taken (i.e., if a silicon disc was bombarded uniformly under controlled conditions, then the resistivity changes at its center were different from those at its edge). By incorporating geometrical correction factors in measuring resistivities more sensible results could be obtained. Tables 1 and 2 show some of the measurements which were done on silicon samples.

Results of the bombardment on the gold layers on the silicon samples were consistent which was an indication of the uniformity of the ion beam. The changes in resistivity of the bombarded gold layers (see Table 3) were most likely resulted from stain on the surface of the sample caused by bombardment under undesirable conditions (e.g., high pressure in the system, or not heating the sample during the bombardment).

5.5 Radiation Damage

In this section we shall focus attention upon the possible disruptions which are brought about in a target under ion bombardment. The removal or reduction of radiation damage is the most important aspect of ion implantation, since otherwise the properties of the material are likely to be dominated by the many defects that each ion will produce in coming to rest. Complexities

TABLE 1

RESISTIVITY OF DISCRETE BOMBARDED CIRCULAR AREAS ON SILICON

(After cleaning in HF)

Current (mA)	Voltage (V)	Resistivity (ohm-cm)
10	1.138	113.8
100	7.800	78.0
10*	1.540	154.0
50*	5.771	115.4
100*	10.730	107.3

* Same area.

TABLE 2

RESISTIVITY OF BOMBARDED SILICON AREA BETWEEN DEPOSITED Au LAYER

Current (mA)	Voltage (V)	Resistivity (ohm-cm)
10	0.0143	1.430
100	0.1447	1.447
200	0.2942	1.470

TABLE 3

RESISTIVITY OF DEPOSITED Au LAYER ON SILICON AFTER BOMBARDMENT

(Resistivity of Unbombarded Au = 0.006 ohms-cm)

Current (mA)	Voltage (V)	Resistivity (ohm-cm)
25*	0.0045	0.180
50*	0.0091	0.183
10**	0.0014	0.140
50**	0.0070	0.140
100**	0.0137	0.137
200**	0.0280	0.140
10	0.0014	0.140

* Same area.

** Same area.

in understanding of radiation effects to semiconductor materials(or devices) arise from the numerous possible combinations of different types of radiation, radiation damage, and semiconductor materials (or devices) affected by radiation. However, understanding and predicting the damaging effects of radiation in semiconductor materials (or devices) does not require a detailed knowledge of the radiation. The problem of predicting many different radiation effects is greatly simplified by characterizing the radiation by its effect rather than by the radiation type, intensity, and energy distribution[18].

Changes in the electrical behavior of semiconductor devices are due to two fundamental effects of radiation in semiconductor material, displacements and ionization. Displacement is referred to any physical damage to a crystal lattice produced by knocking an atom from its normal lattice position to another location in the lattice, or in other words the interactions of ions and crystal atoms. The displacement of an atom from a lattice site into a nearby interstitial position further results in a combination of a vacancy and an interstitial, which is known as "point" defect or Frenkel pair. These defects introduce additional states in the energy gap and can act as additional recombination centers which cause a reduction in the minority carrier lifetime, or they may act as additional impurities that change the net impurity concentration.

The second effect is ionization, which may be defined as the knocking of orbital electrons from an atom to form ionized atoms and free electrons. This interaction results in two types of radiation damage in semiconductor materials (or devices): transient damage effects, and surface damage effects[18]. Transient damage effects in silicon materials are produced by hole-electron pair generation, a result of ionizing characteristic of radiation. The

term transient effects as used here is restricted to the transient changes in the electrical properties of a device due to ionization in the bulk semiconductor material.

In this chapter operations of the experimental ion implantation system were first discussed and described. Second, the results of experiments along with measurements were investigated. Finally, a discussion of probable radiation damages was given. In the final chapter of this paper the future work of ion implantation along with some advantages of ion implantation in device fabrication will be discussed.

CHAPTER VI

CONCLUSION

From the result of tests conducted on the ion source it became certain that the system could give ion beams over considerable periods (45 minutes) provided that there was no cause for arcing or voltage breakdown in the system. Toward the end of a filament's lifetime the current needed to produce a particular ion current fell slowly presumably because the filament diameter was being reduced by oxidation of the tungsten to volatile tungsten oxide, a catastrophic process in the final stages leading to burning-out of the filament. It is probable that the black powder coating the inside of the source after some hours operation is thus mainly tungsten oxide. This coating could be removed fairly easily with a mild abrasive cleaning powder and hot water.

Results of some initial experiments from ion implantation in rock salt crystals indicated that the energies to which ions were accelerated were sufficient to give the ions the power to penetrate into crystals. This was confirmed by the formation of "bubbles" inside the rock salt crystal after it was bombarded with nitrogen ions. In the case of ion implantation in silicon, though the "formation" of a p-n junction was not achieved, the results showed some resistivity changes which in turn indicated some structural changes in the silicon. These changes could have been entirely due to structural damage as a consequence of (i) the high dose ion bombardment, (ii) not heating

the target while it was being bombarded, (iii) and no post bombardment annealing. There has been some speculation that having a large area junction ($\sim$ 1.0 cm^2 in this case) lowers to near zero the probability of finding a successful junction. Even a very tiny "bad" region in the crystal could effectively short out the junction. Typical active areas on most common devices is a square 30 to 100 mils on a side.

It has been demonstrated that ion implantation when properly employed is an effective means of introducing impurity atoms into single-crystal semiconductor materials. The advantages of the ion implantation techniques in the field of semiconductor (silicon) technology may be briefly summarized as follows. It is possible by means of ion implantation to accurately control impurity concentration profiles in very narrow regions (less than 1μ) near the silicon surface. The formation of buried impurity layers could be used in simplifying the construction of certain devices (i.e., FETs). The ability to bombard over metal as well as oxide masks might be used to advantage in integrated circuit technology in the fabrication of complex device structures. Because of its greater control over impurity concentration profiles the construction of "diffused" resistors as employed in integrated circuits is possible by changing sheet resistivity values[20]. Nonthermal distributions of various impurities within semiconductor materials, which is perhaps the greatest contribution of ion implantation, result in the following additional advantages. Since impurity ions diffuse only into regions of a semiconductor material not covered with masks on the surface this reduces the junction capacitance which is a critical parameter at high frequencies. The breakdown voltage of a junction can also be improved if the junction is produced by ion implantation technique.

One problem, which is of great importance, that the author, as well as a majority of investigators in this field, has come across is the difficulty of making any meaningful measurements on the implanted materials. Because the extent of implanted layers is limited, therefore, the problem of determining material properties always requires measurements on very thin film of limited extent. This tends to be a serious problem, especially if the film resides on an electrically active material of any great thickness[20].

In the experimental system used by the author the apparatus is presently being modified so that samples can be heated (up to temperatures > 600°C) during implantation. It should now be possible to (a) eliminate most of the undesirable contamination effects and (b) to anneal out some of the lattice damage produced by implantation. The specimen will be heated on the face away from the impinging ion beam by placing it at a focus of a parabolic reflector containing a 650 watt quartz-iodine lamp at the other focus. The apparatus is being constructed from stainless steel plate and alumina support rods to form a separate "optical bench" array behind the specimen.

REFERENCES

1. Kittel, C.
   Introduction to Solid State Physics, John Wiley, (1968)

2. Sze, S. M.
   Physics of Semiconductor Devices, John Wiley, (1969)

3. Azaroff, L. V.
   Introduction to Solids, McGraw-Hill, (1960)

4. Girifalco, L. A.
   Atomic Migration in Crystals, Blaisdell Publishing Co., (1964)

5. Smith, R. A.
   Semiconductors, Cambridge University Press, (1959)

6. Neuberger, M.
   "Germanium Data Sheets", DS-143
   Hughes Aircraft Co., Feb. 1965
   Culver City, California

7. Brophy, J. J.
   Semiconductor Devices, McGraw-Hill, (1964)

8. Strutt, M. J. O.
   Semiconductor Devices, Vol. 1, Academic Press, (1966)

9. Daughety, D. G. and H. E. Talley
   Physical Electronics,
   (To be published 1969)

10. Large, L. N.
    Contemp. Phys. 10 277, (1969)

11. Ohl, R. S.
    Bell System Tech. J. 31 104, (1952)

12. Bohr, N.
    Kgl. Danske Vid. Selsk. Matt.-Fys.
    Medd. 18 # 8, (1948)

13. Lindhard, J., M. Scharff, and H. E. Schiott
    Kgl. Danske Vid. Selsk. Matt.-Fys. Medd.
    33 # 14, (1963)

14. Lindhard, J.
Kgl. Danske Vid. Selsk. Matt.-Fys. Medd.
34 # 14, (1965)

15. Gibbons, J. F.
Proc. IEEE 56 # 3, (March 1968)

16. Klemperer, O.
Electron Optics, Cambridge University Press, (1953)

17. Liebmann, G.
Proc. Phys. Soc. 62 (B) 213, (1949)

18. Larin, F.
Radiation Effects in Semiconductor Devices,
(Ch. 1 & 9) John Wiley, (1968)

19. Dearnaley, G.
Rep. Prog. Phys. 32 405, (1969)

20. Kleinfelder, W. J.
SEL Tech. Rep. K701-1
Stanford University, (1967)

ACKNOWLEDGMENT

The author wishes to express his sincere appreciation to Professor Derek J. Stirland for his guidance and assistance throughout the course of the investigation and preparation of this paper. Financial support for the project was provided by the Organized Research Program at Kansas State University, Department of Electrical Engineering.

APPENDIX A

AVERAGE SQUARE FLUCTUATIONS

Average energy loss per unit path length may be defined by

$$\frac{dE}{dR} = N \cdot S = N \int T d\sigma \qquad \text{(A-1)}$$

Also, from Eq. 15 the average square fluctuation in energy loss is

$$(\overline{\Delta E})^2 = N \cdot dR \int T^2 d\sigma \qquad \text{(A-2)}$$

The average square fluctuation in range (range "straggling") as given by Lindhard et al[13] is

$$(\overline{\Delta R})^2 = \int \frac{N \cdot \Omega^2(E)}{(dE/dR)^3}\, dE = \frac{1}{N^2} \int \frac{\Omega^2(E)}{S^3(E)}\, dE \qquad \text{(A-3)}$$

where

$$\Omega^2(E) = \frac{(\overline{\Delta E})^2}{N \cdot dR} = \int T^2 \cdot d\sigma \qquad \text{(A-4)}$$

$$S(E) = S_e(E) + S_n(E) \qquad \text{(A-5)}$$

In the above equations T is the energy transfer to atoms and atomic electrons, $S_e(E)$ and $S_n(E)$ are the electronic and nuclear stoppings which may be obtained in the following manner. From Eqs. 16a and 16b one may write

$$S_n(E) = \left(\frac{dE^*}{dR^*}\right)_n \tag{A-6}$$

$$S_e(E) = k \cdot (E^*)^{\frac{1}{2}} \tag{A-7}$$

where E* and R* can be obtained as follows

$$E^* = E \frac{aM_2}{z_1 z_2 e^2 (M_1 + M_2)} \tag{A-8}$$

$$R^* = RN \frac{4\pi a^2 M_1 M_2}{(M_1 + M_2)^2} \tag{A-9}$$

where

$$a = (0.8853) \cdot a_0 (z_1^{2/3} + z_2^{2/3})^{-\frac{1}{2}} \tag{A-10}$$

in which a_0 is the Bohr radius, z_1 and z_2 are the atomic numbers, M_1, M_2 are the atomic masses of the incident and the host atoms, respectively, and the constnat 0.8853 is the Thomas-Fermi constant.

The differential scattering cross section may also be obtained in the following manner

$$d\sigma = \pi a^2 \frac{dU}{2U^{3/2}} f(U^{\frac{1}{2}}) \tag{A-11}$$

where

$$U^{\frac{1}{2}} = E^* \cdot \sin(\psi/2) \quad . \tag{A-12}$$

The angle ψ is the deflection from the axis of incidence (see Figs. 3-4 and 3-5). For elastic collisions one may obtain the following relation

$$\mathrm{Sin}^2(\psi/2) = \frac{T}{T_m} \qquad \text{(a-13)}$$

where T and T_m are the energy transfer and its maximum value, respectively, in a collision with an atom at rest.

SOME STUDIES OF ION IMPLANTATION AT LOW ENERGIES

by

IRAJ ROJHANI

B. S., Kansas State University, 1969

AN ABSTRACT OF A MASTER'S THESIS

submitted in partial fulfillment of the

requirements for the degree

MASTER OF SCIENCE

Department of Electrical Engineering

KANSAS STATE UNIVERSITY
Manhattan, Kansas

1970

ABSTRACT

An investigation of the performance of a commercial ion source for future use in a 600 KV Cockcroft-Walton accelerator has been carried out: A major part of the experimental work involved determining the optimum conditions for producing a focused ion beam (using an Einzel lens array).

Argon and nitrogen ions have been implanted into rock salt (sodium chloride) crystal and p-type silicon at low energies (< 20 KV). The effects of implantation in rock salt have been studied by optical microscopy and in silicon some preliminary measurements of electrical properties have been made.

These preliminary results and future studies are discussed in this report.